Commercial Scale CO_2 Injection and Optimization of Storage Capacity in the Southeastern United States

Final Scientific/ Technical Report

Reporting Period: January 2013 – October 2017

Principal Authors: George Koperna, Principal Investigator,
Advanced Resources International

Dr. Jack Pashin,
Oklahoma State University

Dr. Peter Walsh,
University of Alabama, Birmingham

Report Date: October 27, 2017

DOE Cooperative Agreement: DE-FE00110554

Submitted by: Advanced Resources International, Inc.
4501 Fairfax Drive, Suite 910
Arlington, VA 22203

Oklahoma State University
Boone Pickens School of Geology
Noble Research Center
Oklahoma State University
Stillwater, OK 74078

University of Alabama – Birmingham
School of Engineering
1075 13th Street South, Suite 101
Birmingham, Alabama 35294-4440

Disclaimers

U.S. Department of Energy

This report was prepared as an account of work sponsored by an agency of the United States Government. Neither the United States Government nor any agency thereof, nor any of their employees, makes any warranty, express or implied, or assumes any legal liability or responsibility for the accuracy, completeness, or usefulness of any information, apparatus, product, or process disclosed, or represents that its use would not infringe privately owned rights. Reference herein to any specific commercial product, process, or service by trade name, trademark, manufacturer, or otherwise does not necessarily constitute or imply its endorsement, recommendation, or favoring by the United States Government or any agency thereof. The views and opinions of authors expressed herein do not necessarily state or reflect those of the United States Government or any agency thereof.

Advanced Resources International, Inc.

The material presented in this report is intended to support the objectives of this specific application only. Any use of this material in relation to any other specific application should be based on independent examination and verification of its unrestricted applicability for such use and on a determination of suitability for the application by professionally qualified personnel. No license under any Advanced Resources International, Inc., patents or other proprietary interest is implied by the publication of this application. Those making use of or relying upon the material presented in this application for any other purpose, assume all risks and liability arising from such use or reliance.

Abstract

The Commercial Scale Project is a US DOE/NETL funded initiative aimed at enhancing the knowledge-base and industry's ability to geologically store vast quantities of anthropogenic carbon. In support of this goal, a large-scale, stacked reservoir geologic model was developed for Gulf Coast sediments centered on the Citronelle Dome in southwest Alabama, the site of the SECARB Phase III Anthropogenic Test.

Characterization of regional geology to construct the model consists of an assessment of the entire stratigraphic continuum at Citronelle Dome, from surface to the depth of the Donovan oil-bearing formation. This project utilizes all available geologic data available, which includes: modern geophysical well logs from three new wells drilled for SECARB's Anthropogenic Test; vintage logs from the Citronelle oilfield wells; porosity and permeability data from whole core and sidewall cores obtained from the injection and observation wells drilled for the Anthropogenic Test; core data obtained from the SECARB Phase II saline aquifer injection test; regional core data for relevant formations from the Geological Survey of Alabama archives. Cross sections, isopach maps, and structure maps were developed to validate the geometry and architecture of the Citronelle Dome for building the model, and assuring that no major structural defects exist in the area. A synthetic neural network approach was used to predict porosity using the available SP and resistivity log data for the storage reservoir formations. These data are validated and applied to extrapolate porosity data over the study area wells, and to interpolate permeability amongst these data points. Geostatistical assessments were conducted over the study area.

In addition to geologic characterization of the region, a suite of core analyses was conducted to construct a depositional model and constrain caprock integrity. Petrographic assessment of core was conducted by OSU and analyzed to build a depositional framework for the region and provide modern day analogues. Stability of the caprock over several test parameters was conducted by UAB to yield comprehensive measurements on long term stability of caprocks.

The detailed geologic model of the full earth volume from surface thru the Donovan oil reservoir is incorporated into a state-of-the-art reservoir simulation conducted by the University of Alabama at Birmingham (UAB) to explore optimization of CO_2 injection and storage under different characterizations of reservoir flow properties. The application of a scaled up geologic modeling and reservoir simulation provides a proof of concept for the large scale volumetric modeling of CO_2 injection and storage the subsurface.

Table of Contents

List of Figures

List of Tables

Acronyms and Abbreviations

ADEM	Alabama Department of Environmental Management
AoR	area of review
CO_2	carbon dioxide
ft	feet (1 ft = 0.3048 m, 1 ft^3 = 0.0283168467117 m^3)
km	kilometer (1 mile = 1.609344 km, 1 square mile = 2.58998811 km^2)
m	meter
μm	micron, micrometer (1 μm = 10^{-6} meter)
mD	millidarcy (1mD = 0.001 darcy, 1mD = 9.869233E-16 m^2)
mm	millimeter (1 mm = 10^{-3} meter)
MPa	megapascal (1MPa = 1,000,000 Pa)
MW	megawatt
MVA	Monitoring, verification and accounting
NaCl	sodium chloride
OSU	Oklahoma State University
ΔP	change in pressure
Pa	pascal, measure of pressure equivalent to 1 Newton of force per $meter^2$, N/m^2
pH	measure of the hydronium ion concentration in aqueous solutions, which determines the acidity or basicity of a solution
ppm	parts per million
psi	pounds per square inch; measure of pressure (14.696 psi = 1 atmosphere; 1 psi = 6894.76 pascal)
SECARB	Southeast Carbon Sequestration Partnership
S_g	gas saturation
S_w	water saturation
tonnes	metric tons (1,000 kg)
tons	short tons (2,000 lbs)
UAB	University of Alabama at Birmingham
UIC	Underground Injection Control
USDW	underground source of drinking water

Executive Summary

The US DOE/NETL funded Commercial Scale project aims to enhance the knowledge base and technical ability of industries to geologically store vast quantities of anthropogenic carbon. For this project, a large-scale, stacked reservoir geologic model was developed for estimating potential storage volumes in the specific, well constrained geologic terrane Gulf Coast sediments centered on the Citronelle Dome in southwest Alabama, the site of the SECARB Anthropogenic Test.

A detailed geologic model of the full earth volume from surface through the Donovan oil reservoir is incorporated into a state-of-the-art reservoir simulation conducted by the University of Alabama at Birmingham (UAB) to explore optimization of CO_2 injection and storage under different characterizations of reservoir flow properties. In conjunction with geologic modeling, a suite of core analyses was performed to assess and model long-term caprock stability. These data contribute to advancement of the science, assisting industries' ability to predict CO_2 storage capacity within ±30%, develop and validate technologies to ensure 90% storage permanence, and to improve reservoir storage efficiency while ensuring containment.

To develop the geologic model, a robust geologic assessment was conducted for the study area. The characterization work includes: 1) A generalized regional geologic characterization; 2) application of a neural network to extrapolate petrophysical parameters from vintage raster log data; and 3) geostatistical approaches. These are used to populate the model with data and to place constraints on the subsurface storage potential. Together, these provide the framework for model development. Characterization of regional geology to construct the geologic model consists of an assessment of the entire stratigraphic continuum of the Citronelle Dome, from surface to depth of the Donovan oil-bearing formation. This project utilizes all available geologic data available, which includes: modern geophysical well logs from three new wells drilled for SECARB's Anthropogenic Test; vintage logs from the Citronelle oilfield wells; porosity and permeability data from whole core and sidewall cores obtained from the injection and observation wells drilled for the Anthropogenic Test; core data obtained from the SECARB Phase II saline aquifer injection test; regional core data for relevant formations from the Geological Survey of Alabama archives. Cross sections, isopach maps and structure maps were developed to validate the geometry and architecture of the Citronelle Dome for building the model, and assuring that no major structural defects exist in the area. A synthetic neural network approach was used to predict porosity using available SP and resistivity log data for the storage reservoir formations. These data were validated and applied to extrapolate porosity data over the study area wells, and to interpolate amongst these data points. Geostatistical assessments were conducted over the study area.

In addition to geologic characterization of the region, a suite of core analyses was conducted to construct a depositional model and constrain caprock integrity. Oklahoma State University research suggests that the Paluxy Formation caps a major transgressive-regressive cycle during the Lower Cretaceous. Core analyses indicate that the Paluxy represents a coarsening-upward succession composed of numerous stacked, aggradational sandstone-mudstone packages. Sedimentological analysis demonstrates that the Paluxy Formation was deposited in a continental environment that included bedload-dominated fluvial systems and interfluvial paleosols. Several modern analogues of the Paluxy formation are proposed here from interpretations of the petrographic and geophysical data.

Additional research was conducted on assessing the stability of the caprocks in the geologic continuum. Caprock samples from Paluxy core taken from the SECARB Anthropogenic Test site were tested by UAB to yield comprehensive measurements on long term stability of caprocks.

The reservoir simulation of the Commercial Scale project study area was designed to assess a baseline, pre-injection pressure assessment and a post-injection pressure distribution for several heterogeneity and injection scenarios to ascertain the impact on the geologic continuum in terms of the interrelated injectivity, storage capacity and efficiency, as well as geomechanical effects. The Paluxy sandstone was designated as the target baseline sandstone to benchmark all injectivity scenarios. The other reservoirs selected for injection and storage assessment include the Washita, the Lower Tuscaloosa and the Wilcox Formations.

The simulation protocol consisted of three principal injection scenarios: 1) Initial standalone injection into each unique sand body; 2) Sequential injection into two reservoirs (dual injection scenario); and 3) Sequential injection into four reservoirs (quad injection scenario). Injection into each reservoir is conducted for a duration of 40 years – therefore, the dual sequential injection scenario spans an 80-year period, and the quad injection scenario spans a 160-year period.

The application of a scaled up geologic modeling and reservoir simulation provides a proof of concept for the large scale volumetric modeling of CO_2 injection and storage the subsurface. Other key findings include:

- The initial reservoir simulation shows negligible difference between the high heterogeneity and low heterogeneity cases. Possible explanations are that the very high permeability of these Gulf Coast sandstone reservoirs minimizes the effect of reservoir heterogeneity and/or the approach used to generate the high heterogeneity and low heterogeneity cases using different contouring methods for porosity maps was inadequate for the high permeability reservoirs at Citronelle Field. This finding warrants further investigation to fully characterize the impact of impermeable and very low permeability depositional and diagenetic features that are observed to be present from core and logs. Such features would include caliche zones, shale layers, abandoned channel fill, tight carbonates and cemented sandstones.

- The prior injection into one formation appears to have no significant impact upon injectability into adjacent formations in multi-sequence injections. This finding suggests that the high porosity and high permeability Gulf Coast sediments rapidly dissipate any injection induced pressure build-up over the study area, but this finding warrants further investigation to fully characterize the pressure effects of sequential injection into multi-stacked reservoirs at lower permeability values.

1.0 Introduction

1.1 Study Objectives

The objective of this study was to explore the potential optimization of commercial CO_2 injection and storage within a vertical geologic continuum from depth to surface in the Gulf Coast region of the southeastern United States. The Gulf Coast region is underlain by a massive "wedge" of predominately clastic deposits that spans the region and thickens basin ward into Gulf of Mexico geologic basin. Consequently, a thick sequence of potential CO_2 storage reservoirs and sealing formations will be present at any potential storage site selected in the Gulf Coast region. Such storage sites would most likely be selected because of favorable geologic structure for trapping injected CO_2. Because geologic structure and reservoir characteristics favorable for the long-term storage of CO_2 are also favorable for the trapping and accumulation of oil and natural gas, future commercial CO_2 injection and storage sites are likely to also be sites of producing or depleted oil and gas fields. This affords an opportunity to apply the geologic data available from oil and gas production fields to develop the thorough characterization of potential storage volumes that will be needed to implement CO_2 storage at a commercial scale.

The Commercial Scale CO_2 Injection project leverages the site-specific geologic data available for the SECARB Phase III Anthropogenic Test site at Citronelle Field in Mobile County, Alabama to fully quantify and optimize the storage capacity and injectivity of each reservoir unit at the site. The potential sub-surface storage volume occurs from a depth of approximately 12,000 vertical feet to surface, and over a geographic area of more than 56 square miles.

The three main components of the project were:

- Development of a detailed geologic model of the full earth volume from surface through the Donovan oil reservoir and three reservoir heterogeneity cases for Citronelle Field.
- Reservoir simulation of commercial scale CO_2 injection for the low and high reservoir heterogeneity cases to determine total storage volumes and reservoir storage efficiency.
- Application of an economic cost model to assess the life cycle cost of commercial scale storage operations.

Each project component is discussed in a following chapter of this report. Two additional studies were completed as part of the geologic model analysis. These include:

- Laboratory measurement and simulation of caprock integrity performed by the University of Alabama – Birmingham (UAB), and
- Analysis of the depositional systems of the Paluxy formation at Citronelle field performed by Oklahoma State University (OSU).

Results of these associated studies are reported in the Appendices.

1.2 Study Area Background

The Citronelle Dome is a well-documented hydrocarbon trap in southwest Alabama – the target of oil production from the Donovan formation sandstones since 1955 (Eaves, 1976). The site, shown in **Figure 1,** was chosen for the SECARB Phase III Anthropogenic Test, a large scale, fully-integrated CO_2 injection demonstration project (Koperna et al., 2013). During the Anthropogenic Test, 114,000 tons of CO_2 captured from Alabama Power's Plant Barry, were transported via 12 miles of pipeline and injected at Citronelle oil field (Koperna et al., 2013). The CO_2 was injected into a deep saline reservoir, the Paluxy formation, at a subsea depth of approximately 9,400 feet.

A thorough geologic characterization of the Citronelle Dome was conducted for the SECARB Phase III Anthropogenic Test. **Figure 2** is a structure map of the Citronelle Dome showing the outline of Citronelle field and the location of the Anthropogenic Test Site. The amalgamation of all available geologic data demonstrates the presence of structural closure at all stratigraphic horizons to the surface (Esposito et al, 2008). This project established that sufficient pore volume and injectivity existed at the project site, with numerous additional storage horizons accessible (Esposito et al, 2008).

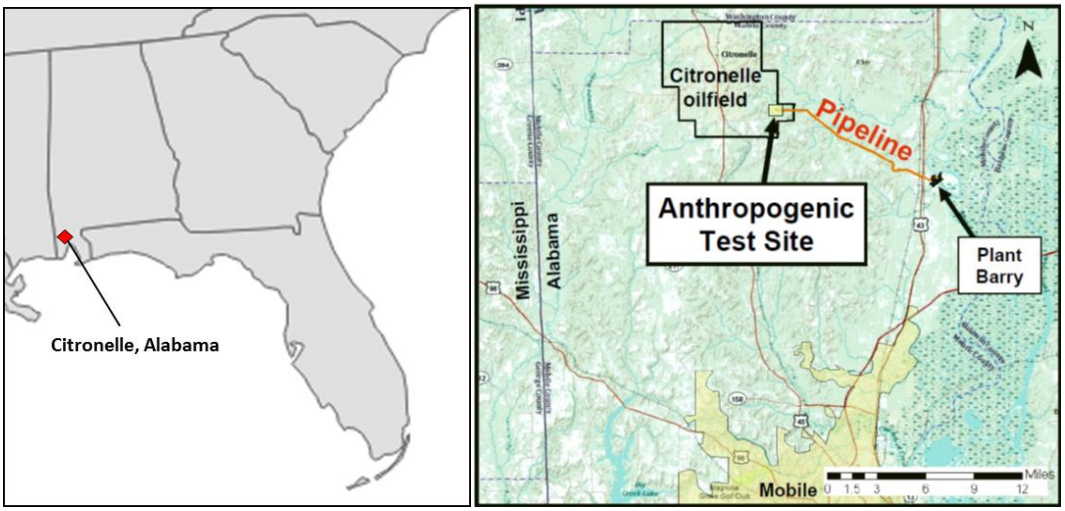

Figure 1: Map showing location of Citronelle in Alabama and the location of Plant Barry (from Pashin et al., 2008)

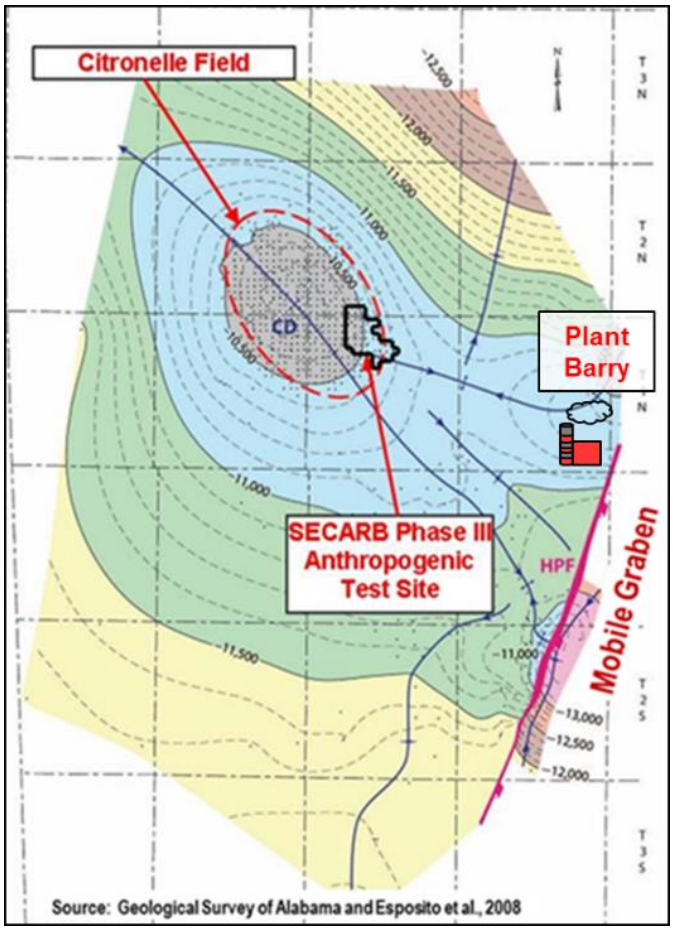

Figure 2: Geologic structure map of Citronelle Dome in Alabama, showing the location of Citronelle field and the Anthropogenic Test site and regional structural features. Contour interval is 100 feet. (from Esposito et al., 2008)

2.0 Geologic Model of Citronelle Field

2.1 Geologic Characterization

An upscaled model of the area was built for multiple geologic formations to establish sufficient pore volume and potential injectivity to contain commercial volumes of CO_2. Construction of the geologic model was predicated upon the characterization of geologic features for each stratigraphic horizon from surface through the base of the productive Donovan Formation. These features included structural elevation, porosity, permeability and stratigraphic continuity.

To build the large scale geologic model, a regional geologic assessment of Citronelle was conducted to select study area boundaries, and complete a spatial characterization of the attributes of all stratigraphic horizons within the study area. Essential information includes the thickness, lateral continuity, porosity and permeability of target reservoirs, sealing horizons, and other intervening layers. **Figure 3** shows the a 56 mi^2 Commercial Scale Project study area, outlined in red; the Citronelle field outline in light blue; and the three injection and observation wells drilled for the SECARB Phase III Anthropogenic Test.

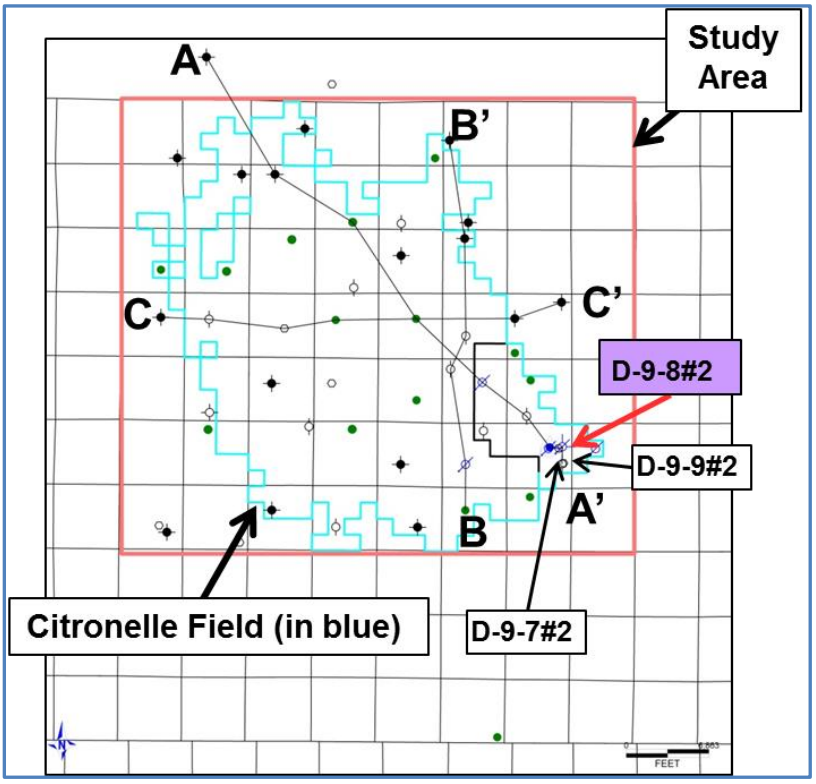

Figure 3: Study Area for Geologic Model of Citronelle Field

The geologic characterization of the Citronelle Field study area determined that: 1) the storage reservoirs and their associated confining units are both continuous and laterally extensive; 2) no major faults appear to cut across the study area; 3) the geologic structure of the Citronelle Field

is a simple dome ideal for trapping CO_2 and stratigraphic closure is present at all stratigraphic horizons; and 4) the storage reservoirs exhibit heterogenous reservoir characteristics.

2.1.1 Geologic Data Applied to the Development of the Model

The geologic assessment conducted for the Commercial Scale project utilized a host of available and geologic data. These data include:

- Geophysical well logs from three new wells drilled for SECARB's Anthropogenic Test;
- Well logs from the Citronelle oilfield wells;
- Porosity and permeability data from whole core and sidewall cores obtained from the injection and observation wells drilled for the Anthropogenic Test;
- Core data for the Tuscaloosa, Eutaw and Selma formations obtained from the Plant Daniel SECARB Phase II saline aquifer injection test (Koperna et al, 2009);
- Regional core data for relevant formations from the Geological Survey of Alabama;
- Cross well seismic surveys and vertical seismic profiles from the Anthropogenic Test wells

The geologic characterization included: 1) a generalized regional geologic characterization of the geologic formations present at Citronelle field; 2) application of a neural network analysis to extrapolate petrophysical parameters from raster log data for legacy wells at Citronelle field; and 3) geostatistical assessment of stratigraphic continuity and reservoir heterogeneity (Esposito et al., 2008; Koperna et al., 2012; Petrusak et al. 2009).

A database was established of over 80 well logs in the Citronelle field using IHS Petra Software. Applying findings from Pashin et al., (2008), the stratigraphy was correlated over the entire study area to constrain the extent of all stratigraphic horizons. A suite of structure maps, isopach maps and cross sections were generated to provide assessments of structural integrity of the formations and the lateral extent of target injection horizons and cap rocks.

The simple structural geometry of the salt-cored dome is illustrated by the structure maps for each interval. This is made evident by the shallowing of formation tops centered on the axis of the dome, which increases in depth concentrically outwards from the center of the field. An example is shown in **Figure 4b**. The thickness data derived from log correlations applied here are shown in **Table 1**. Three cross-sections (**Appendix A**) traversing the Citronelle oilfield demonstrate both the lateral extent of each stratigraphic unit throughout the study area, and the absence of faults. It should be noted that while not all stratigraphic units are of consistent thickness over the study area, they remain present throughout.

The maps and cross sections developed for this project verify the location and geometry of the Citronelle Dome. The geospatial stratigraphic data aggregated provides the structural framework necessary to build the dimensional component of the large-scale geologic numerical model.

Table 1: Stratigraphic Interval Thickness

Stratigraphic Unit		Unit Thickness (Feet)			Unit Designation
		Minimum	Maximum	Mode	
Lower Wilcox		490	650	580	Potential Reservoir
Midway		700	880	800	Confining
Selma		1,070	1,380	1,175	Confining
Eutaw	Total	210	310	245	Potential Reservoir
	Tombigbee Sand	30	85	60	
Tuscaloosa	Upper Tuscaloosa	502	618	555	Potential Reservoir
	Marine Tuscaloosa	180	360	290	Potential Reservoir
	Marine Shale	65	190	100	Confining
	Pilot Sand	88	130	111	Potential Reservoir
	Lower Tuscaloosa	220	350	283	Potential Reservoir
Washita-Fredericksburg	Washita	630	1,260	980	Potential Reservoir
	Fredericksburg	960	1,200	1,060	Lower Confining Shale (averages 200 ft. thick)
Paluxy		1,090	1,185	1,140	Potential Reservoir
Mooringsport		210	320	240	Confining
Ferry Lake		50	70	60	Confining

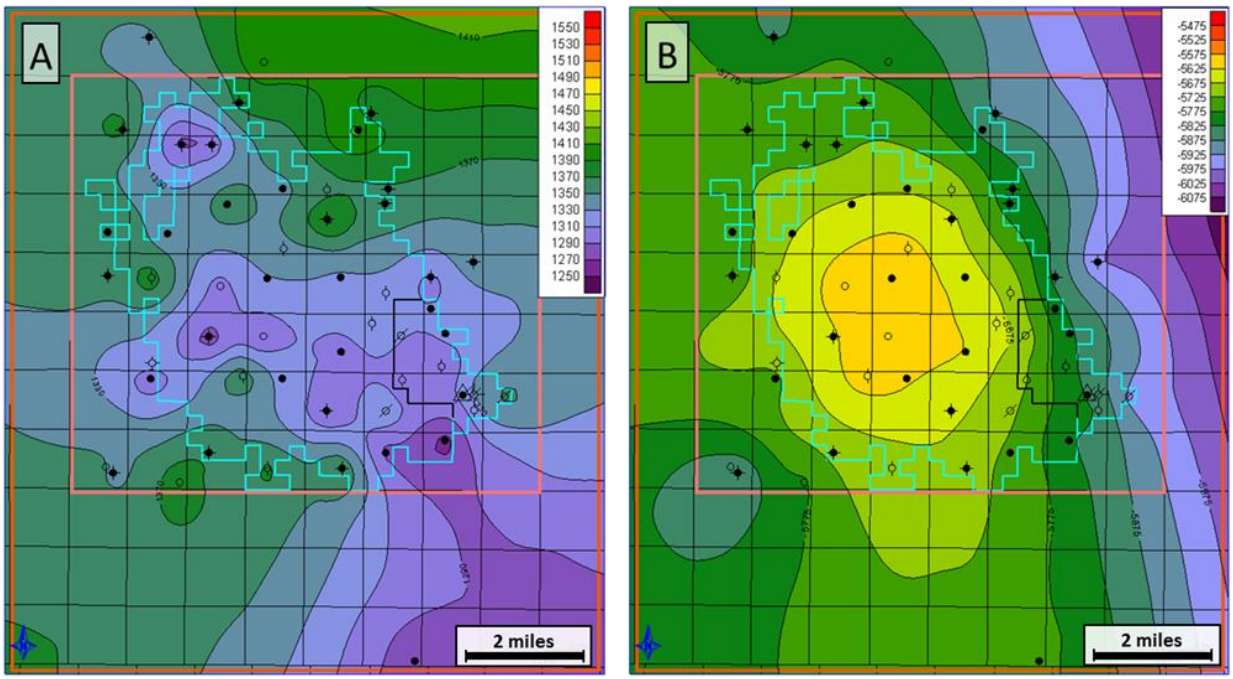

Figure 4: An isopach map showing thickness (Fig 4a) and a structure map (Fig. 4b) of the Tuscaloosa Group over the Citronelle Field study area. Contour interval for Fig. 4a is 20 ft. Contour interval for Fig. 4b is 50 ft.

In addition to the geospatial and dimensional geologic data, porosity and permeability data are necessary to build a robust geologic model for numerical simulation. Porosity and permeability data are essential for assessing the injectivity, storage volumes for CO_2 containment, and flow characteristics of potential storage reservoirs. The publicly available petrophysical data measured from regional cores and core date collected for the SECARB Anthropogenic test were applied here. These provide partial coverage of the data necessary for several key reservoirs in the stratigraphic succession to populate the Petra database. **Tables 2a** and **2b** provide porosity and permeability data from regional core analyses as described by Pashin et al., (2008). However, these data are limited and do not allow for a robust analysis of reservoir properties over the entire study area on their own.

Table 2a: Regional Core Porosity and Permeability

Stratigraphic Unit		Core Porosity (%)			Core Permeability (mD)		
		Minimum	Maximum	Mean	Maximum	Mean	Median
Selma		11.8	16.6	14.9	0.03	0.01	0.01
Eutaw		10.2	39.7	24.8	5,470	184	35
Upper Tuscaloosa		13.8	35.1	25.2	1,520	225	76
Lower Tuscaloosa	Pilot Sand	8.7	40.0	24.6	2,840	206	74
	'Massive' Sand	12.5	38.6	26.1	1,773	269	125
Washita-Fredericksburg		15.1	32.0	24.6	863	184	164
Paluxy		12.3	29.4	23.3	3,950	131	131

Notes: All data from Pashin et al., (2008)

Table 2b: Core Porosity and Permeability Data from SECARB Phase II and Phase III Tests

Stratigraphic Unit		Porosity (%)			Permeability (mD)		
		Minimum	Maximum	Mean	Maximum	Mean	Median
Lower Tuscaloosa	'Massive Sand'	17.8	26.1	22.5	2314.0	692.9	657.0
Paluxy Formation		5.5	24.7	17.5	3897.0	52.2	118.0

2.1.2 Predicting Porosity with Synthetic Neural Networks

For most of the legacy wells in Citronelle Field, the only available logs include vintage spontaneous potential logs (SP) and induction electric resistivity logs collected from the 1950's through early 1970's. Most wells lack porosity logs needed to extrapolate CO_2 injectivity and volume capacity for the storage reservoirs. To compensate for the lack of porosity logs, synthetic porosity log curves were generated from induction electrical logs using neural network software. The Citronelle D 9-7 #2 and D-9-8 #2 wells drilled for the SECARB Phase III Anthropogenic Test, and the resistivity logs from their paired offset wells, the D 9-7 #1 and D 9-8 #1, were used to "train" a neural network to generate synthetic density porosity logs from the vintage resistivity logs. The synthetic porosity logs were validated using core data plus the modern density-neutron porosity logs from the D 9-9 #2 observation well drilled for the Anthropogenic Test. The neural net approach was then applied to generate synthetic density porosity curves for a study dataset of 33 legacy Citronelle wells.

Synthetic neural networks are a well-established method for pattern recognition, providing a tool to extrapolate truth-grounded synthetic data for a related data set (Hopfield, 1982; Bishop, 1995). Research at West Virginia University (e.g. Mohaghegh, 2000) has focused on utilizing neural networks to solve petroleum engineering challenges. The application of neural networks for the Commercial Scale CO_2 Injection project provided an opportunity to use existing well logs to predict porosity for individual study wells, and to interpolate the predicted porosity over the entire Study Area (Jonsson et al., 2013; MacGregor et al., 2014).

This neural network approach was possible because three new wells were drilled for the SECARB Anthropogenic Test on the same well pads as existing abandoned wells (distances ranging to less than 300 feet away). The setup and application of a neural network for this study utilizes the data from three pairs of new and abandoned wells in the Citronelle Southeast Unit. The well pairs include: 1) the D-9-7 #1 (old well) and the D-9-7 #2 (new),158 feet apart; 2) the D-9-8 #1 (old) and the D-9-8 #2 (new), 318 feet apart; and 3) the D-9-9 #1 (old) and the D-9-9 #2 (new), 105 feet apart. For each new well, a suite of modern logs was collected which included porosity measurements. The close stratigraphic correlation of each new-well/old-well pair provided an excellent opportunity to use neural network software, by applying SP and resistivity logs as proxies for porosity. Application of this technique assumed that there is negligible difference in gross lithology or physical characteristics between the closely paired wells in each old well-new well pair.

A neural network was trained to use these data to compute the known porosity of the modern well. The data used to develop the neural network includes the spontaneous potential (SP), induction (IL) and short normal (SN) curves from the abandoned wells, and the sandstone density porosity log from the new wells. An example well log is provided in **Figure 5**. By training the SP and resistivity log on the associated porosity value obtained from modern logs, an algorithm can be developed to predict porosity. The trained neural network was then used for the prediction of porosity from data in new and legacy adjacent wells. Comparison of these data with the actual values measured in the new wells validated the efficacy of this method.

The two-step process of training, followed by validating the neural network is essential to ensure the quality of the synthetic neural network prediction. The neural network was then used to predict porosities from the log data available for other legacy wells throughout the study area. These data are intended for porosity data extrapolation over study area wells, and interpolation amongst these data points to generate model grids.

The results of the trained neural network yielded robust validations. **Figure 6** shows the comparison of the D 9-9 #1 (vintage raster data) and the D 9-9 #2 (modern well log suite). The third track represents the density porosity measurement for the D 9-9 #2 and the synthetically derived porosity for the 9-9 #1. The porosities predicted for key reservoirs including the Eutaw Tombigbee Sandstone, Tuscaloosa, Washita-Fredericksburg and Paluxy are in relative agreement. Porosity is predicted where it is anticipated from geologic assessment, and the predicted values agree with measured values as shown in **Figure 7.** It should be noted that vertical resolution from the neural network logs is not as well delineated as it is in the actual logs which show a more jagged “sawtooth” appearance. **Figure 7** shows that the predicted and actual average porosity values for the Paluxy sandstones are very close for the D-9-9 #1 and #2 well pair. There is a larger range between minimum and maximum values and finer vertical resolution for actual porosity than for the predicted porosity.

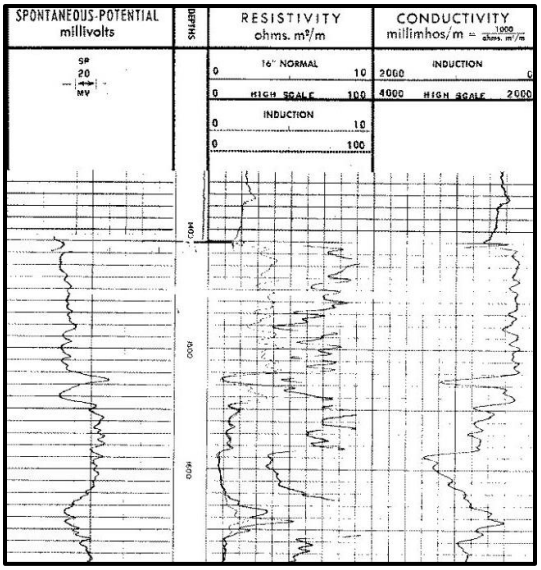

Figure 5: Vintage Raster Log Sample from the Citronelle Oil Field, Well D 9-8 #1

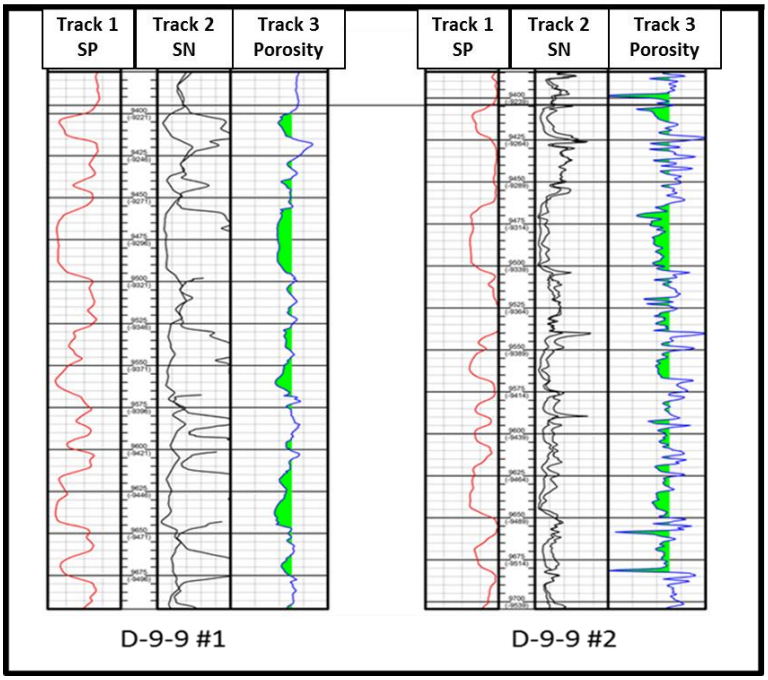

Figure 6: Post Training Validation of D-9-9#1 Synthetic Porosity Compared to the D-9-9 #2 Actual Porosity in the Upper Paluxy Formation. Green Shading Indicates Porosity Greater than 15 Percent. SP Indicates Spontaneous Potential Log and SN Indicates the Short Normal Resistivity Log.

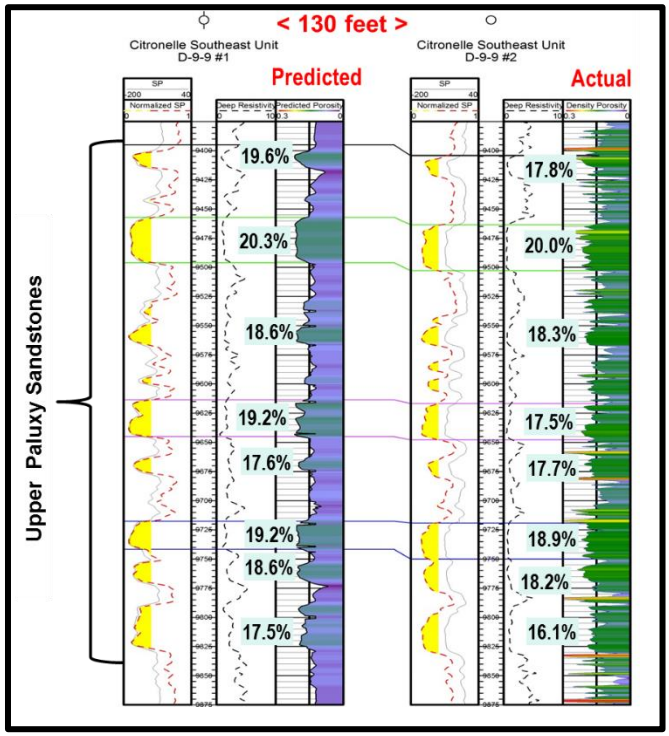

Figure 7: Comparison of Neural Net Predicted and Measured Porosity for Selected Upper Paluxy Sandstones in D-9-9 #1 and D-9-9 #2 Wells

The trained and validated neural network was applied to 36 wells throughout the study area to generate a synthetic suite of predicted density porosity curves. These predicted porosities were applied to interpolate porosity amongst each study well and to establish the total pore volume for the geologic model. The following are examples of neural network outputs for one of the study wells, the A-34-6 #1, which is located approximately 5.5 miles from the D-9-9 #1 as shown in **Figure 8.**

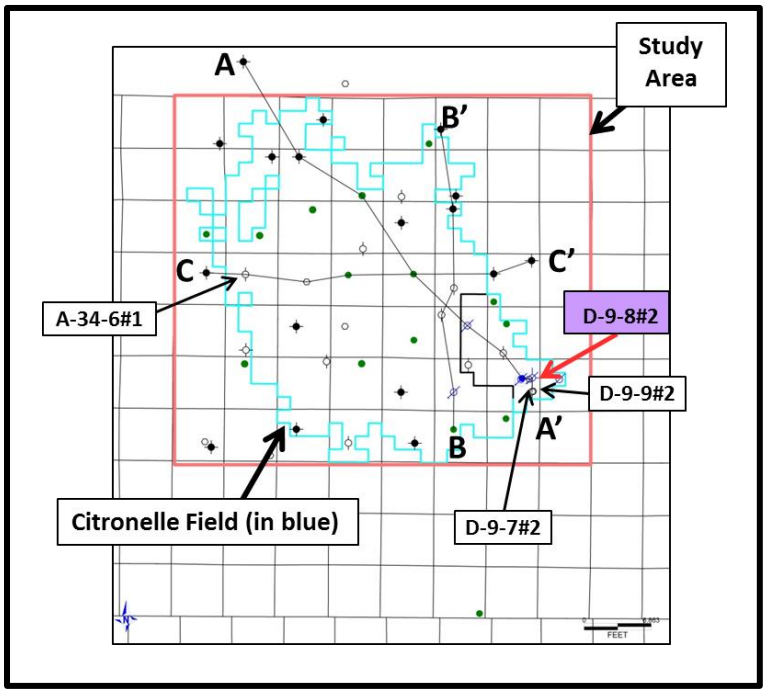

Figure 8: Study Wells for Porosity Prediction using Neural Networks

Figure 9, 10 and 11 are examples of neural net predicted porosity for the selected sandstones in the A-34-6 #1 well. Normalized SP log is shown on the first (left hand) track with the sandstones highlighted in yellow. Deep resistivity is plotted in the middle track on a linear scale from 0 ohmm to 10 ohmm. Predicted density porosity is shown in the right hand track. The scale is fraction porosity of 0.4 on the left and 0 on the right. The predicted porosity curve is geoshaded to highlight subtle porosity variations and to provide a quick visual connection to the sandstones highlighted on the SP curve. Average synthetic porosity is shown for selected sandstones indicated on each figure. In this case, there is no offset well with which to compare predicted and actual porosity. However, the predicted porosity values for the study wells can be compared to the regional core data. For the Tuscaloosa, Washita-Fredericksburg, and Paluxy Formation examples shown in Figure 9, 10 and 11, the predicted porosity values correspond appropriately to the range of known core porosity values for the study area and vicinity that are provided in **Table 2** (Jonsson, et al 2013; MacGregor et al., 2014).

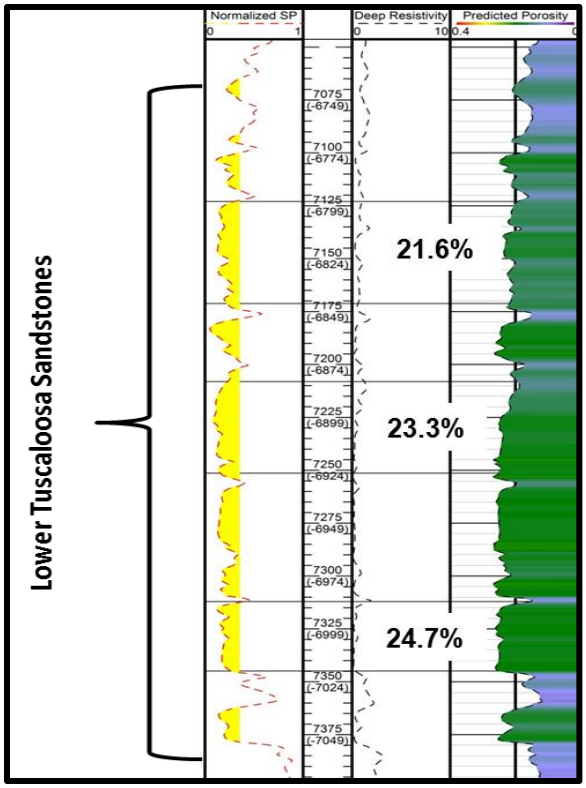

Figure 9: Predicted Porosity for Selected Lower Tuscaloosa Sandstones in the A-34-6 #1 Well

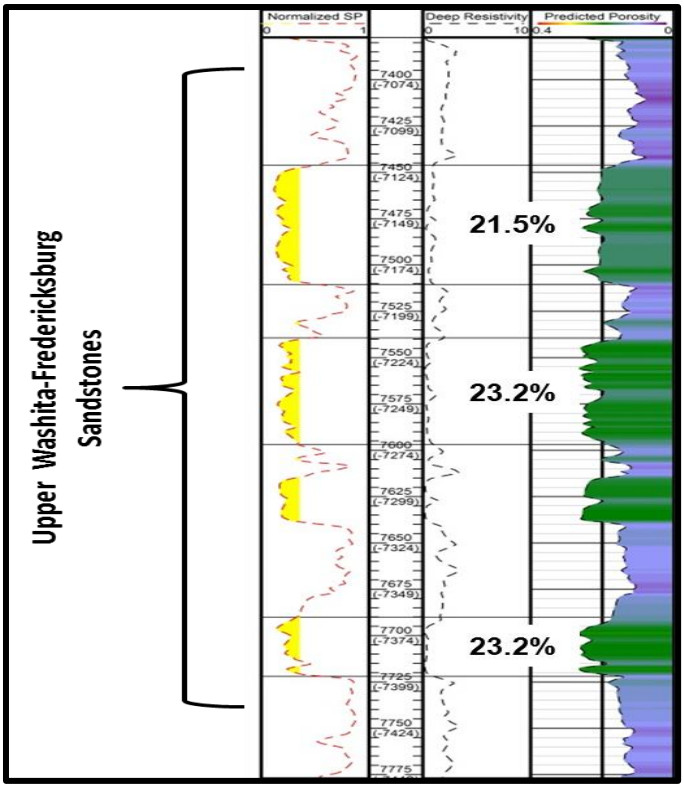

Figure 10: Predicted Porosity for the Selected Upper Washita-Fredericksburg Sandstones in the A-24-6 #1 Well

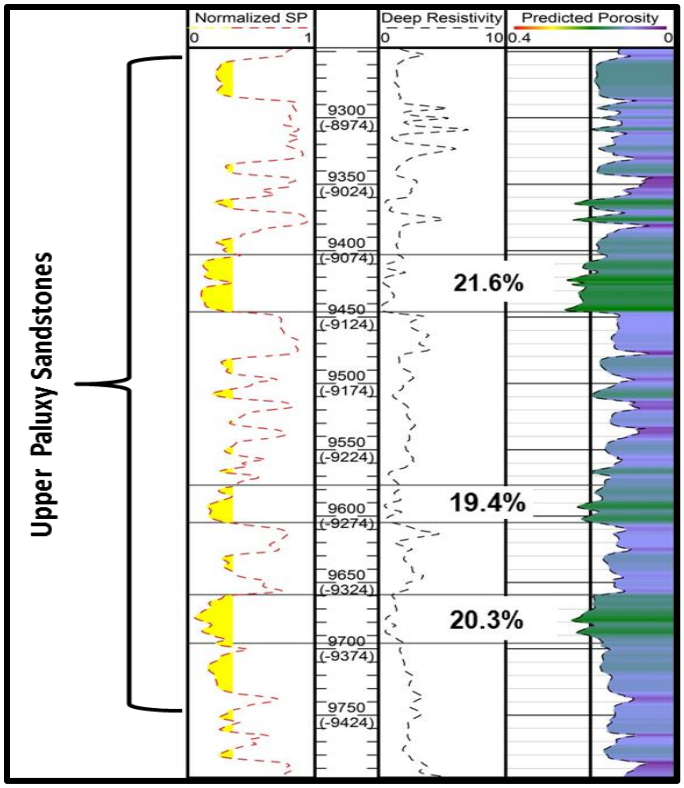

Figure 11: Predicted Porosity for Selected Upper Paluxy Sandstones in the A-34-6 #1 Well

2.1.3 Permeability Transforms

To interpolate porosity over the study area, the correlation of porosity and permeability from core analyses collected for the SECARB Phase III Anthropogenic Test was conducted. A positive linear correlation was extrapolated between the porosity and permeability data from these analyses within a formation. Regression analyses were performed by a comparison of the $\log_{10}$ of permeability to porosity, which resulted in coefficients of determination (R^2) ranging from 0.61 to 0.85. The formula relating the two parameters was then applied to estimate the permeability from predicted porosity determined from neural network analysis of selected sandstone formations. **Figure 12** illustrates a permeability transform of the Anthropogenic Test's target injection zone, and **Table 3** shows examples of permeability values extrapolated from porosity, based upon the core porosity-permeability transform. Yellow shading in **Table 3** indicates the range of porosity values observed in the core data, where the non-shaded values are outside the observed range.

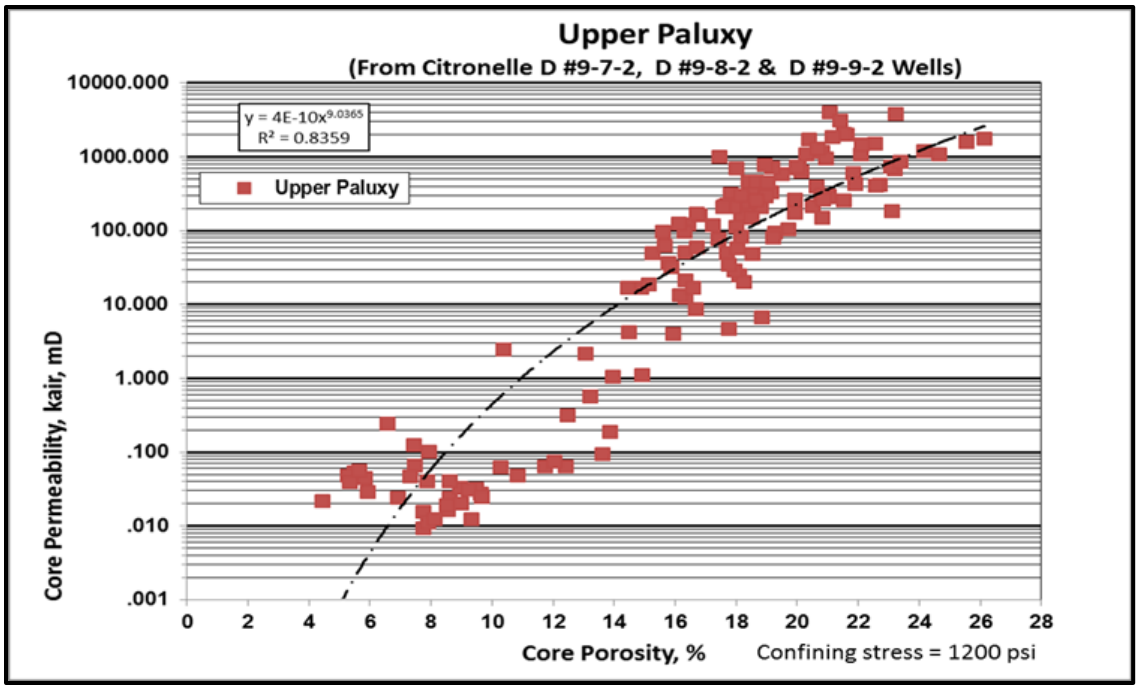

Figure 12: Upper Paluxy Permeability Transform Determined from Core Date Obtained from The SECARB Phase III Anthropogenic Test Observation and Injection Wells

Table 3: Examples of Permeability Values Extrapolated from the Upper Paluxy Core Porosity-Permeability Transform

Core Porosity, %	Upper Paluxy Core Permeability, mD	Core Porosity, %	Upper Paluxy Core Permeability, mD
6	0.004	24	1,186.7
8	0.058	26	2,446.1
12	2.26	28	4,778.6
16	30.4	30	
20	228.5	32	
22	540.6	34	

2.2 Geologic Model for Reservoir Simulation

2.2.1 Geologic Model Structure

A 400-layer, finite element model was generated using the Computer Modelling Group's *GEM* software. The model is comprised of 4.8 million cells: 120 cells in the 'X' direction; 100 cells in the 'Y' direction; and 400 cells in the 'Z, direction. The grid block dimensions are 500 feet x 500 feet in the 'X' and 'Y' directions. The model area is 56 square miles and the model thickness is 12,000 vertical feet, or 2.27 miles, yielding a geomodel volume of 127.12 miles^3 or 1.87e^{13} ft^3.

Model cells are defined by geologic data interpreted from well logs, including model layer thickness, depth and geographic position. Associated petrophysical data for each cell, porosity and permeability, were obtained from measured data and extrapolated from the neural network analysis. The data were input into the Petra database to develop the geologic model. To build the 'upscaled' reservoir simulation model, the geologic and petrophysical data assessed for this project were aggregated into discrete layers that extend over the entire study area. Data were interpolated over the study area by applying a kriging model, which generated study maps for every attribute of each model layer.

2.2.2 Geologic Model Layers

The entire volume of the study area, from ground surface to the Donovan Formation (12,000 vertical feet) is divided into 400 layers or "flow units". **Table 4** summarizes the number of layers defined for each stratigraphic interval, the permeability values or permeability transform assigned to each stratigraphic interval, the interval designation as either a potential reservoir or confining unit. The geologic structure (defined by thickness and depth) and the flow properties (defined by porosity and permeability) were characterized for each layer. Permeability transforms are shown in **Table 4** where data were available. If insufficient log data were available at Citronelle Field, model layer attributes were extrapolated from regional data.

Table 4: Summary of Stratigraphic Intervals and Model Layers in Commercial Scale Geologic Model

Formation	# Model Layers	Permeability Transform	Formation Designation
Alluvium	**1**	500,000 mD	Too Shallow / USDW
Citronelle	**1**	17,500 mD	Too Shallow / USDW
Miocene	**1**	34,600 mD	Too Shallow / USDW
Chickasawhay	**1**	1,100 mD	USDW
Vicksburg	**1**	0.032 mD	Confining
Jackson	**1**	0.032 mD	Potential Confining
Claiborne	**3**	0.032 to 386 mD	Potential Confining
Wilcox	**5**	3.09E-5 to 660 mD	Confining
Midway	**5**	3.24E-6 to 1,680 mD	Potential Confining
Selma	**20**	$K = 0.0033(e^{(0.1735*\phi)})$	Confining
Eutaw	**20**	$\text{Log } k = (0.13*\phi)-1.56$	Potential Storage Reservoir
Upper Tuscaloosa	**50**	$\text{Log } k = (0.18*\phi)-2.92$	Storage Reservoir
Tuscaloosa Marine Shale	**10**	$k = (6E-19)*(\phi^{12.52})$	Confining
Lower Tuscaloosa	**30**	$k = (2E-14)*(\phi^{12.176})$	Storage Reservoir
Washita	**60**	$k = (1E-9)*(\phi^{8.257})$	Storage Reservoir
Fredericksburg	**60**	$k = (1E-9)*(\phi^{8.257})$	Potential Storage Reservoir
KWF Confining	**5**	1.21E-4 mD	Confining
Upper Paluxy	**60**	$k = (4E-10)*(\phi^{9.0365})$	Storage Reservoir
Lower Paluxy	**20**	$K = 0.0004(e^{(0.6242*\phi)})$	Storage Reservoir
Mooringsport	**5**	$K = 0.0033(e^{(0.1735*\phi)})$	Confining
Ferry Lake Anhydrite	**1**	5.5E-05 mD	Confining
Donovan	**40**	$K = 0.002(e^{(0.4873*\phi)})$	Storage Reservoir

Upscaling of geologic data for the potential CO_2 storage horizons is intended to provide finer resolution of reservoir flow properties. The injection and storage horizons with the best characteristics are subdivided into more model layers as shown in **Table 5**. For example, the Upper and Lower Cretaceous formations (Selma through the Donovan) are divided into the most layers because the Cretaceous section contains the most promising CO_2 injection targets, has very good log coverage, and substantial core data available in several formations. The layer flow characteristics are extrapolated from measured data.

Potential confining horizons are characterized at lower resolution than CO_2 injection and storage horizons, which means fewer and thicker layers, and relatively uniform layer flow characteristics.

Low priority storage horizons may be shallow, have thin- or discontinuous reservoirs, and less favorable flow characteristics. Flow characteristics of the layers are estimated, or extrapolated from more remote geologic data sources (such as geologic publications) rather than direct core measurements. For example, the Lower Tertiary (Claiborne through Midway) is divided into fewer, coarser layers. No valid porosity logs are available and most of the logs in the data set were not run through the upper Wilcox and Claiborne formations. Each shallow formation from the Upper Eocene Jackson Group to ground surface is represented as a single layer in the model, and single values of thickness, porosity and permeability are applied to the layer throughout the entire study area.

Accurately representing the storage capacity and flow properties of the reservoir, namely reservoir porosity and permeability, is integral to upscaling the geologic model. For the geologic section from the Upper Cretaceous age Selma Group through the Lower Cretaceous age Donovan Formation, each model layer is represented for individual study wells by single point values for average thickness, porosity, and depth. Geostatistical approximations are used to interpolate layer thickness, and porosity between study wells and throughout the study area. Series of grid maps are created for each model layer with datum for layer thickness, average porosity, and sand/ shale extent. Porosity permeability transforms derived from actual core data are then applied to these porosity grids to provide a corresponding up-scale of reservoir flow properties for each model layer.

For the geologic section from the base of surface casing (generally in the Tertiary age Wilcox Formation) through the top of the Selma Group, geophysical well logs are available in all study wells. However, poor geophysical data were historically collected for these strata. Therefore, synthetic porosity logs derived from the neural net analyses are not valid for the Tertiary geologic section in the study area. Instead, SP-resistivity logs are used to upscale the model layers to correspond to published stratigraphic divisions and depositional features of the Tertiary geologic section. No direct log porosity data are available, so single average porosity and permeability values, which are based on published data, are assigned to each model layer

Table 5: Example of Detailed Model Layer Attributes at Citronelle Field

Formation	Layers	Average Layer Thickness	Minimum Layer Thickness	Maximum Layer Thickness
Lower Tuscaloosa	30	9.5 feet (2.9 meters)	8.1 feet (2.5 meters)	12 feet (3.7 meters)
Washita	60	16.2 feet (5.0 meters)	13.4 feet (4.1 meters)	18.9 feet (5.8 meters)
Upper Paluxy	60	10.5 feet (3.2 meters)	8 feet (2.4 meters)	12.5 feet (3.8 meters)
Upper Donovan	40	11.5 feet (3.5 meters)	9.5 feet (2.9 meters)	13.1 feet (4.0 meters)

2.3 Geostatistical Analysis

A geostatistical analysis of all sedimentary formations represented in the Citronelle Field is essential to establishing realistic ranges of data in the geologic model. Key petrophysical attributes were extrapolated for each geologic model layer over the study area using the Petra software tool – e.g. porosity, thickness, structural elevation. Data from the modern well logs and neural network were evaluated utilizing a geostatistical approximation to place constraints on porosity and permeability, thereby constraining potential storage capacity and flow properties in the reservoir simulation.

The geostatistical analysis provided three geomodels for simulating the range of the CO_2 storage potential present in each geologic formation from surface to the base of the Donovan oil-producing sandstones. Ranges were established by individually assessing each model layer for three unique reservoir heterogeneity scenarios: a "base" control scenario; a" high" reservoir heterogeneity scenario; and a "low" reservoir heterogeneity scenario.

2.3.1 Reservoir Heterogeneity Scenarios

Grids for three heterogeneity scenarios for each layer were generated in *Petra*. These scenarios include; 1) a "base" or intermediate heterogeneity case; 2) a high heterogeneity case, and 3) a low heterogeneity case. The maps provide a range of values for the petrophysical parameters controlling the study area. Each map utilized a unique surface style contouring package in Petra, summarized in **Table 6,** to yield each heterogeneity scenario. These surface contouring styles are designed to extrapolate porosity and permeability data for the injection and confining horizons, which allows predicted porosity data to be interpolated across the study area, and the generation of associated permeability values for the geologic model. **Figures 13, 14 and 15** show examples of the maps generated for each heterogeneity scenario which were used to spot check and validate the geostatistical analysis.

Table 6: Heterogeneity Scenario Information for *Petra*

Heterogeneity Scenario	Surface Style Contouring
Base Case	Highly connected features
Low Heterogeneity	Minimum Curvature
High Heterogeneity	Disconnected Features

Three scenarios of porosity heterogeneity are incorporated into the geologic model for each layer. **Figure 13** through **Figure 15** show maps produced for three layers in the Upper Paluxy, and one layer from the Lower Tuscaloosa, the Washita, and Upper Donovan Formations. A low heterogeneity case and high heterogeneity case are compared to the control, or "base case" to

provide a range for reservoir heterogeneity. Heterogeneity increases from left to right, which is noted by the more discontinuous contours with greater heterogeneity.

The maps visually detail the potential heterogeneity of the storage reservoirs and confining units on a layer by layer basis. In each instance, the connectivity of contours tends to diminish from the low to high heterogeneity case. The low heterogeneity scenario is commonly depicted with large regions of similarly connected porosity values, while the high heterogeneity maps show highly isolated contours. The base case provides an intermediary heterogeneity analysis. These visual representations detail the potential range in reservoir heterogeneity, which will serve as the foundation for the geologic model.

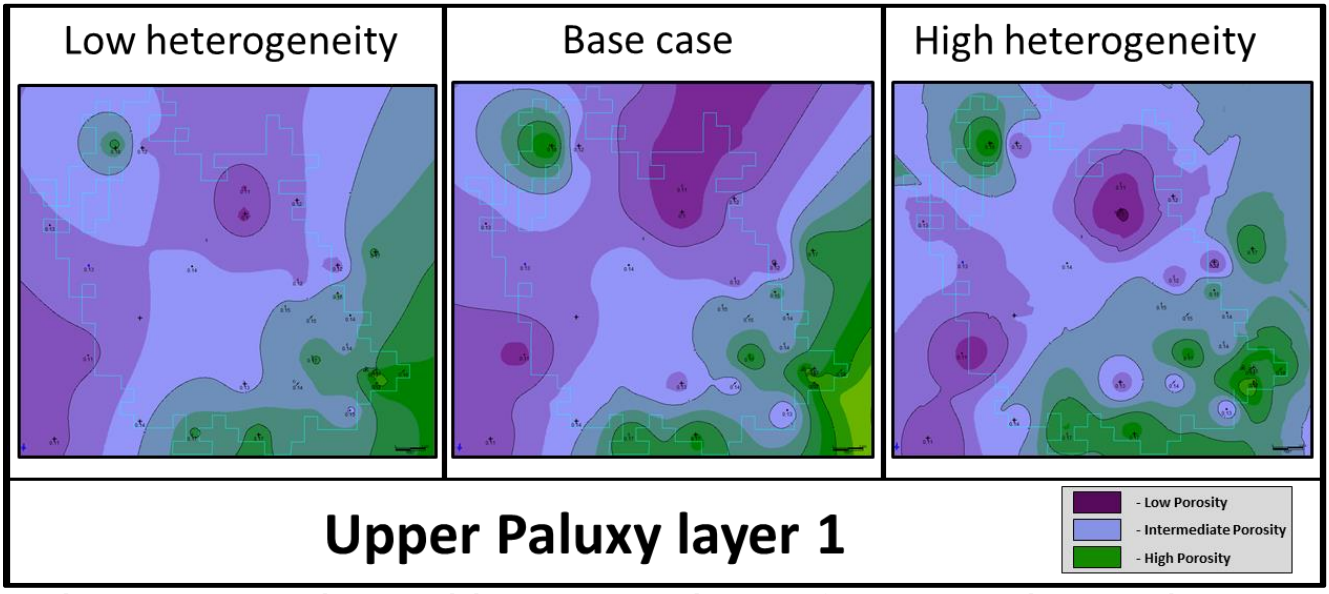

Figure 13: Upper Paluxy, Model Layer 1; Porosity Maps for Heterogeneity Scenarios

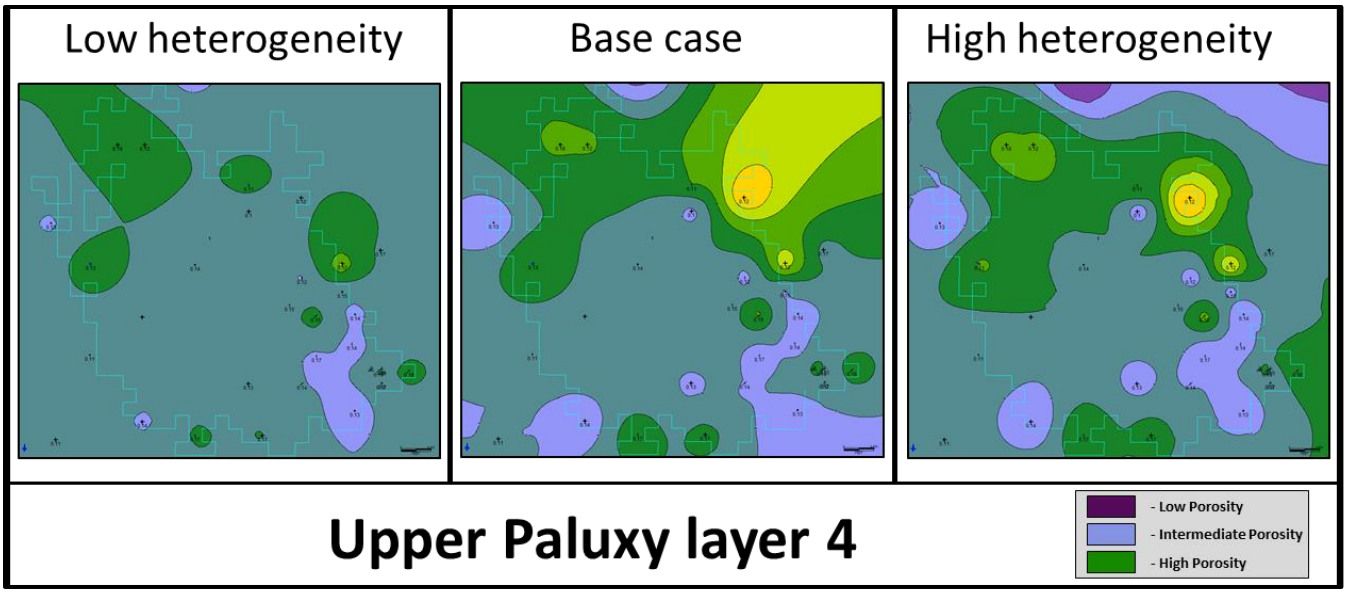

Figure 14: Upper Paluxy, Layer 4; Porosity Maps for Heterogeneity Scenarios

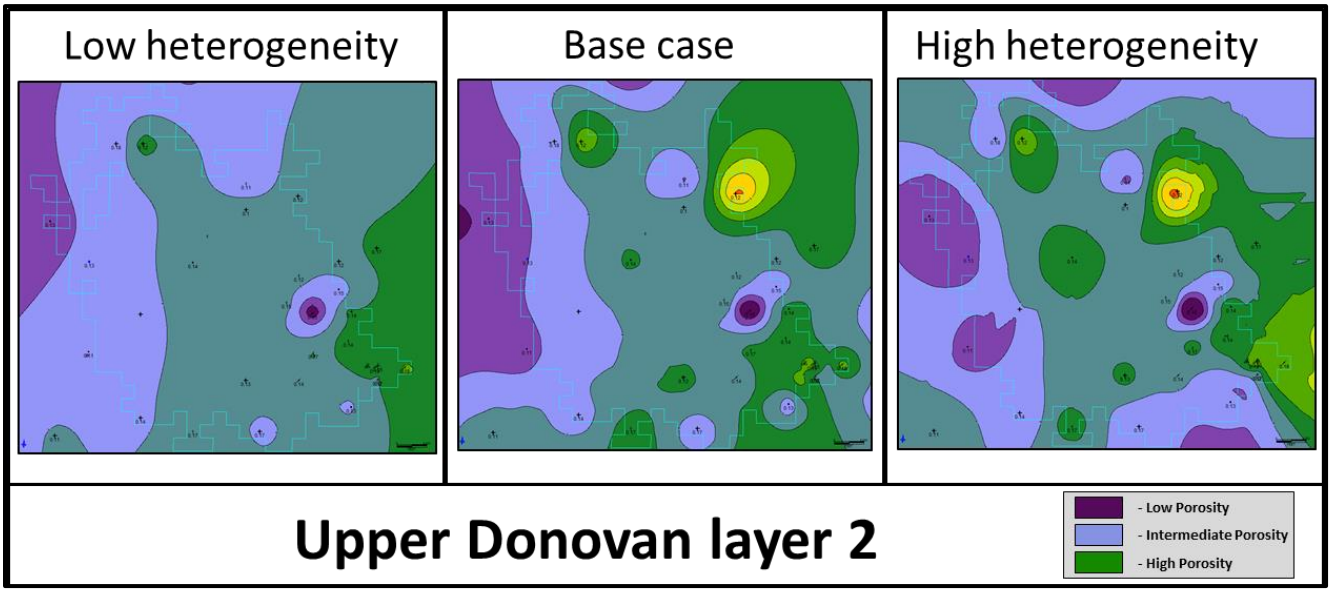

Figure 15: Upper Donovan, Layer 2; Porosity Maps for Heterogeneity Scenarios

3.0 Reservoir Simulation

Once constructed, the geologic model was transferred to UAB's Information Technology Research Computing Laboratory to run the advanced simulations of the geologic model. Each of the 400 layers were incorporated into the Computer Modelling Group's *GEM* reservoir simulator, with three geostatistical scenarios devised for each,

3.1 Reservoir Simulation Protocol

The reservoir simulation was designed to assess a baseline, pre-injection pressure assessment and a post-injection pressure distribution for several heterogeneity and injection scenarios to ascertain the impact on the geologic continuum in terms of the interrelated injectivity, storage capacity and efficiency, as well as geomechanical effects. The Paluxy sandstone was designated as the target baseline sandstone to benchmark all injectivity scenarios. The other reservoirs selected for injection and storage assessment include the Washita, the Lower Tuscaloosa and the Wilcox Formations.

The simulation protocol consists of three principal injection scenarios: 1) Initial standalone injection into each unique sand body; 2) Sequential injection into two reservoirs (dual injection scenario); and 3) Sequential injection into four reservoirs (quad injection scenario). Injection into each reservoir is conducted for a duration of 40 years – therefore, the dual sequential injection scenario spans an 80-year period, and the quad injection scenario spans a 160-year period.

Standalone injections were conducted to establish baseline storage factors for each amenable saline reservoir represented in the geologic continuum in the Gulf Coast sediments represented at the Citronelle study area. The primary focus was the target Paluxy Formation. Injection runs are also conducted for the Washita, the Lower Tuscaloosa and the Wilcox Formations.

The dual injection scenarios were conducted on each potential reservoir in conjunction with the Paluxy sandstones. Injection occurs separately in each formation in sequence for 40 years, for a total duration of 80 years. The quad injection scenario was conducted on the Upper Paluxy, Washita, Lower Tuscaloosa and Wilcox Formations in sequence. Injection into each formation occurred for a 40-year interval in succession from deepest to shallowest over a 160-year span. These simulation runs were designed to observe any linkage between the storage capacity and sequential injection. Note, no effort was made to discern long-term plume stabilization rates due to a lack of well-understood dissolution and mineralization rates within these formations.

3.2 Comparison of Heterogeneity Cases

For each injection scenario, both single and sequential, two unique heterogeneity cases of the multi-variant injection protocols were conducted to place constraints upon the potential commercial scale injectability of the region. These were a low heterogeneity and a high heterogeneity case for each injection scenario. These provide sensitivity data on the impact of

reservoir heterogeneity on the injectability of each reservoir, yielding insight into the potential range of injection volumes that may result from reservoir variability.

Reservoir simulation results are presented in **Tables 7, 8, 9, 10** and **11** for each injection scenario. These tables delineate: 1) the total volume of pore space available for a defined area; 2) the total volume of that pore space occupied by CO_2; 3) and the pore space utilization efficiency as a calculated percent of these two values for both the high- and low heterogeneity cases. Single layer injection values from modeling yield efficiency factors are delineated in **Table 7.**

Table 7: Single Layer Injection Values from Modeling

Formation	High Heterogeneity			Low Heterogeneity		
	Volume of Pore Space (ft^3)	Volume of Pore Space with CO_2 (ft^3)	Pore Space Utilization Efficiency (%)	Volume of Pore Space (ft^3)	Volume of Pore Space with CO_2 (ft^3)	Pore Space Utilization Efficiency (%)
Upper Paluxy	$1.189x10^{10}$	$1.865x10^{9}$	15.7	1.060×10^{10}	1.847×10^{9}	17.4
Washita	1.423×10^{10}	2.227×10^{9}	15.7	1.507×10^{10}	2.213×10^{9}	14.7
Lower Tuscaloosa	1.945×10^{10}	2.449×10^{9}	12.6	1.843×10^{10}	2.448×10^{9}	13.3
Wilcox	2.213×10^{10}	1.623×10^{9}	7.3	2.213×10^{10}	1.623×10^{9}	7.3

Table 8: Dual Injection into the Upper Paluxy and Washita Formations

Formation	High Heterogeneity			Low Heterogeneity		
	Volume of Pore Space (ft^3)	Volume of Pore Space with CO_2 (ft^3)	Pore Space Utilization Efficiency (%)	Volume of Pore Space (ft^3)	Volume of Pore Space with CO_2 (ft^3)	Pore Space Utilization Efficiency (%)
Upper Paluxy	$1.189x10^{10}$	$1.865x10^{9}$	15.7	1.060×10^{10}	1.847×10^{9}	17.4
Washita	1.423×10^{10}	2.226×10^{9}	15.6	1.507×10^{10}	2.213×10^{9}	14.7

Table 9: Dual Injection into the Upper Paluxy and Lower Tuscaloosa Formations

Formation	High Heterogeneity			Low Heterogeneity		
	Volume of Pore Space (ft^3)	Volume of Pore Space with CO_2 (ft^3)	Pore Space Utilization Efficiency (%)	Volume of Pore Space (ft^3)	Volume of Pore Space with CO_2 (ft^3)	Pore Space Utilization Efficiency (%)
Upper Paluxy	$1.189x10^{10}$	$1.865x10^{9}$	15.7	1.060×10^{10}	1.847×10^{9}	17.4
Lower Tuscaloosa	1.945×10^{10}	2.449×10^{9}	12.6	1.843×10^{10}	2.448×10^{9}	13.3

Table 10: Dual Injection into the Upper Paluxy and Wilcox Formations

Formation	High Heterogeneity			Low Heterogeneity		
	Volume of Pore Space (ft^3)	Volume of Pore Space with CO_2 (ft^3)	Pore Space Utilization Efficiency (%)	Volume of Pore Space (ft^3)	Volume of Pore Space with CO_2 (ft^3)	Pore Space Utilization Efficiency (%)
Upper Paluxy	$1.189x10^{10}$	$1.865x10^{9}$	15.7	1.060×10^{10}	1.847×10^{9}	17.4
Wilcox	2.213×10^{10}	1.618×10^{9}	7.3	2.213×10^{10}	1.605×10^{9}	7.3

Table 11: Sequential Injection into Four Formations: Upper Paluxy; Washita; Lower Tuscaloosa; Wilcox

Formation	High Heterogeneity			Low Heterogeneity		
	Volume of Pore Space (ft^3)	Volume of Pore Space with CO_2 (ft^3)	Pore Space Utilization Efficiency (%)	Volume of Pore Space (ft^3)	Volume of Pore Space with CO_2 (ft^3)	Pore Space Utilization Efficiency (%)
Upper Paluxy	$1.189x10^{10}$	$1.865x10^{9}$	15.7	$1.060x10^{10}$	$1.847x10^{9}$	17.4
Washita	1.423×10^{10}	2.226×10^{9}	15.6	$1.507x10^{10}$	$2.213x10^{9}$	14.7
Lower Tuscaloosa	1.945×10^{10}	2.449×10^{9}	12.6	$1.843x10^{10}$	$2.448x10^{9}$	13.3
Wilcox	2.213×10^{10}	1.612×10^{9}	7.3	$2.065x10^{10}$	$1.552x10^{9}$	7.5

3.3 Injection Scenario Discussion

Results of the injection modeling demonstrates several key points. The Paluxy Formation provides the greatest storage efficiency in the single zone injection scenario for the low heterogeneity case. However, the total storage volumes in the Washita and Lower Tuscaloosa are greater than the Paluxy Formation. Storage efficiencies and injection volumes for the Washita and Lower Tuscaloosa are greater than the Paluxy in both the dual- and quad-injection scenarios for each heterogeneity case. In all cases, the Wilcox has the lowest storage volumes and storage efficiencies of the four formations modeled due to its shallow setting.

There is generally little difference between the pore space utilization efficiencies between the low and high heterogeneity cases. For example, the greatest deviation in pore space utilization efficiency measures 1.7% for single zone injection into the Paluxy. Upon conclusion of 40 years of CO_2 injection into the Upper Paluxy Formation, the low heterogeneity case yields an efficiency of 17.4% and the high heterogeneity case an efficiency of 15.7%. Interestingly, the Washita high heterogeneity case performs better than the low heterogeneity case. This is due to slightly better connectivity, and hence permeability, through the vertical section due to more complexity.

In the stacked dual- and quad-injection scenarios, the prior injection into one formation appears to have no significant impact upon injectability into adjacent formations in multi-sequence injections. This finding suggests that the high porosity and high permeability Gulf Coast sediments rapidly dissipate any injection induced pressure build-up over the study area, but this finding warrants further investigation to fully characterize the pressure effects of sequential injection into multi-stacked reservoirs at lower permeability values. For example, **Table 12** shows that upon conclusion of 40 years of injection into the Upper Paluxy Formation, the utilization of its pore space in the low heterogeneity case, is 17.4%. After sitting idle for 40 years, during injection into one of the formations above, the pore space utilization in the Upper Paluxy decreases to 11.4%. The size of the CO_2 plume has increased by 4 percent as indicated by the change in total pore volume containing CO_2. At 120 years after injection into the Paluxy ceases, the low heterogeneity case shows only negligible expansion of the CO_2 plume in the Paluxy while injection is ongoing into three of the formations above it. The utilization of pore space in the Upper Paluxy by injected CO_2 has decreased to 7.9 percent suggesting that the CO_2 plume has become increasingly diffuse and that some of the CO_2 has been sequestered via dissolution.

Appendix A contains two expanded tables showing the complete results to date of the simulations using the upscaled geologic model implemented in CMG/GEM for injection into single and stacked formations in Citronelle Field. As noted above, the **Appendix A** tables show very little difference between the high heterogeneity and low heterogeneity cases for all injection scenarios.

These raw output tables do not consider dissolution or mineralization and reflect values at the end of 40 years of injection for each layer. In single zone cases, the values reflect the end of the injection period. For dual and quad injection cases, only the final injection zone represents storage efficiency after the 40 years of injection, while the remainder reflect storage efficiency

values at the conclusion of the model run. In these cases, dual and single cases were used to build the tables above on a consistent basis.

3.4 Key Findings of the Geologic Model and Reservoir Simulation of the Commercial Scale CO_2 Injection at Citronelle Field

- Proof of Concept – The application of a scaled up geologic modeling and reservoir simulation provides a proof of concept for the large scale volumetric modeling of CO_2 injection and storage the subsurface.

- The initial reservoir simulation shows negligible difference between the high heterogeneity and low heterogeneity cases. Possible explanations are that the very high permeability of these Gulf Coast sandstone reservoirs minimizes the effect of reservoir heterogeneity and/or the approach used to generate the high heterogeneity and low heterogeneity cases using different contouring methods for porosity maps was inadequate for the high permeability reservoirs at Citronelle Field. This finding warrants further investigation to fully characterize the impact of impermeable and very low permeability depositional and diagenetic features that are observed to be present from core and logs. Such features would include caliche zones, shale layers, abandoned channel fill, tight carbonates and cemented sandstones.

- The prior injection into one formation appears to have no significant impact upon injectability into adjacent formations in multi-sequence injections. This finding suggests that the high porosity and high permeability Gulf Coast sediments rapidly dissipate any injection induced pressure build-up over the study area, but this finding warrants further investigation to fully characterize the pressure effects of sequential injection into multi-stacked reservoirs at lower permeability values.

4.0 Economic Cost Model and Potential Impact of Commercial Scale CO_2 Storage

4.1 Economic Cost Model Background

The economic assessment of a large-scale project is the key component to determining whether the project is feasible. An economic cost model was used to assess the potential costs and economic risks associated with commercial CO_2 storage at Citronelle Field. The related risks are based on assumptions defined by Godec (2017). Cost considerations to assess the life cycle costs of the commercial scale CO_2 storage operations include:

- Injection well drilling,
- Well workovers,
- Injection operations,
- MVA requirements,
- Additional ancillary costs.

Actual field costs from SECARB's Anthropogenic Test in were used as the basis for these cost elements, as well as results of studies and field demonstrations of CO_2 storage (Koperna et al., 2014; ARI, 2009).

The economic cost model is based on the CO_2 Saline Storage Cost Model, developed by the U.S. DOE Office of Fossil Energy National Energy Technology Laboratory (NETL).[1] (The design of the NETL CO_2 Saline Storage Cost Model incorporates the regulatory requirements of the EPA's UIC Class VI regulations. The outputs of the DOE-NETL cost model and study suggest that CO_2 storage costs can range from $5 to $20 per tonne depending on the reservoir properties and structural setting (DOE/NETL-2013/1614). In a study by Godec (2017), some cost ranges for onshore saline reservoirs projects were assessed to range from $6.71 per tonne to $12.11 per tonne depending upon the injection rates and regulatory requirements applied.

4.2 Economic Cost Model Assumptions

4.2.1 Capital Costs

The following list details the upfront capital requirements for a large-scale CO_2 injection and storage project based upon cost drivers for the SECARB Anthropogenic Test site:

- Site characterization and FEED studies
- Class VI permitting and GHG MRR subpart RR plan submissions

[1] https://www.netl.doe.gov/research/energy-analysis/analytical-tools-and-data/co2-saline-storage).

- Maximum monitoring area is the radius of the CO_2 plume at the end of the 40-year injection (see Table 3) plus ½ mile (2,640 ft)
- Baseline 3D seismic survey of the entire maximum monitoring area
- Installation of equipment and baseline monitoring of surface deformation (InSAR and tilt)
- Installation of dedicated microseismic monitoring well field and baseline monitoring
- Baseline 3D seismic survey of the entire maximum monitoring area
- Installation of ten dedicated groundwater monitoring wells and baseline monitoring
- Conversion of five existing oilfield wells to in-zone or above-zone monitoring wells
- Baseline cased-hole neutron logs on new injection well and converted wells
- Installation of operational monitoring equipment (surface rates pressure and temperature; compositional monitoring; corrosion monitoring)
- Plug and abandon eight surrounding oil field wells that represent the most likely leakage conduits

It is assumed by the studies here that none of the existing oil field wells could be converted to UIC Class VI CO_2 storage wells due to their vintage (1950s-1960's). Thus, necessitating an entirely new injection well.

4.2.2 Injection Phase Costs

The following cost assumptions are for 40-years of injection

- Class VI and subpart RR reporting
- Continued surface deformation monitoring (InSAR and tilt)
- Repeat 3D seismic survey of the maximum monitoring area every five years
- Continuous microseismic monitoring
- Groundwater monitoring
- Pressure monitoring of in zone and above zone wells
- MITs of injector and monitoring wells every five years
- Operational monitoring (surface rates pressure and temperature; compositional monitoring; corrosion monitoring)
- Time-lapse cased-hole neutron logs on injection well and converted wells every two years
- Injection site and monitoring well site O&M

4.2.3 Post-Injection Costs

The following cost assumptions for a post injection site care period of 50 years:

- Limited Class VI reporting
- Limited surface deformation monitoring (InSAR and tilt)
- Repeat 3D seismic survey of the maximum monitoring area every ten years
- Semi-continuous microseismic monitoring
- Groundwater monitoring

- Pressure monitoring of in zone and above zone wells
- MITs of injector and monitoring wells every ten years
- Limited operational monitoring (surface pressure and temperature; corrosion monitoring)
- Time-lapse cased-hole neutron logs on injection well and converted wells every five years
- Limited injection site and monitoring well site O&M
- Site closure including injection, deep monitoring and groundwater well plugging

The significant cost drivers for each project phase are detailed in **Table 12**:

Table 12: Main Cost Drivers Associated with Injection and Storage of CO_2

Project Phase	Main Cost Drivers	Cost Estimate
Upfront Costs	• Site characterization • Well Drilling • Well conversion	$2.4M $4.3M/ well $1.3M/ well
Injection Phase	• Monitoring Costs	$1.1M
Post Injection Site Care	• Monitoring Costs	$0.4M
Site Closure	• Injection well plugging • Monitoring well Plugging	$0.2M $0.6M

4.3 Estimated Storage Costs for Commercial Scale CO_2 Storage at Citronelle Field

Table 13 shows storage costs estimated for the Commercial Scale CO_2 project ranging from $3.30 to $27.00 per tonne (2016$).

Table 13: Cost Model Results for the Commercial Scale CO_2 Storage Study Area

Formation	Total storage (40 years), MMtonnes	Monitoring Area, acres	Upfront Costs ($$/tonne)	Operating Costs ($$/tonne)	PISC and Closure ($$/tonne)	Total Costs ($$/tonne)
Wilcox	3.6	3,190	$3.40	$15.50	$8.00	**$27.00**
Lower Tuscaloosa	30.9	18,860	$0.60	$3.10	$1.80	**$5.40**
Washita	30.9	4,790	$0.40	$1.90	$1.00	**$3.40**
Fredericksburg	27.2	3,320	$0.50	$2.10	$1.10	**$3.60**
Upper Paluxy	30.9	4,110	$0.40	$1.90	$1.00	**$3.30**

Commercial CO_2 storage in the in the upper and lower Cretaceous formations of Citronelle Field appear to show good economic promise. This is driven primarily by the high pore-volume and

permeability of local strata. A single injection well may be able to inject over 2,000 metric tonnes per day for multiple years with such favorable reservoir characteristics.

Storage costs assessed for the Commercial Scale project in the Cretaceous saline reservoirs range from $3.30 to $5.40 per metric tonne in amenable reservoir conditions. Comparatively, Godec (2017) reported an injection storage cost of $6.71 per tonne for a Gulf Coast representative storage site. This study was conducted on an individual injection well operating at a rate of 2,000 tonnes per day, comparable to the injection rates that the UAB model suggests are achievable for the Cretaceous saline reservoirs (**Table 4**).

The costs defined by Godec (2017) were developed for an "all in" case, consisting of: monitoring a 30,000-acre area, installation of all new injectors, monitoring wells and stratigraphic test wells, and a robust monitoring program (including 3-D, VSP, and cross-well seismic monitoring program). Regardless, under this study's most stringent case, the injectivity of Gulf Coast geologic units results in manageable storage costs.

4.4 Cost Impact of Continued Plume Growth

Plume migration at Citronelle is minimized due to the internal architecture of the regional geology, making some of the monitoring area dimensions and costs manageable. For example, the Washita and Fredericksburg units and the Upper Paluxy formation containing numerous stacked sandstone-mudstone packages (Folaranmi, A.T., and Pashin, J.C., 2014), which allow for a limited spatially constrained plume. The permeability, porosity and internal structures in these stratigraphic horizons help to reduce the extent of the plume, while formations such as the Lower Tuscaloosa suffer from the large monitoring area resulting from a relatively thin injection zone. The Wilcox formation has limited storage capacity due to its low injection pressure limit.

As a sensitivity, plume growth was shown to impact the monitoring area, but total costs appear to be relatively insensitive to an increased monitoring area. The cost associated with doubling the monitoring area at the Commercial Scale project site from 4,110 acres to 8,220 acres was approximately $0.50 per tonne.

4.4.1 Other Potential Cost Impacts

Notable potential costs that were not considered in this study include any potential reservoir pressure control (i.e., water withdrawal for plume management or injectivity/capacity enhancement) or injection/ monitoring well interventions. The potential for CO_2 storage regulatory evolution over the multi-decade timeframe of these types of projects also presents a challenge that could impact costs.

The main economic conclusion for the feasibility of Commercial Scale storage at the Anthropogenic Test Site is that storage costs would be reasonable if CO_2 could be supplied to storage operators for a reasonable transfer price at amenable stacked formation storage complexes similar to the Citronelle Dome.

4.5 CO_2 Storage with Enhanced Oil Recovery

In addition to modeling storage in saline reservoirs over the study area, the oil-bearing Donovan Formation was assessed for its storage potential. Research and operations both confirm that CO_2 may be effectively stored during the enhanced oil recovery (EOR) process (Hill et al., 2013; Azzolina et al., 2015; IEA, 2015; Kovscek and Cakici, 2005; Wong et al, 2013; Kuuskraa and Wallace, 2014.) CO_2 storage with EOR could help defray the costs of commercial scale CO_2 injection and storage in associated saline formations. For this evaluation, several CO_2 EOR scenarios were compared using *CO_2 PROPHET* and ARI's CO_2-EOR Cost Model. Simulations were conducted utilizing properties shown in **Table 14**.

Table 14: Parameters Applied to the CO_2 EOR Modeling for the Donovan

Parameter	Variable
Area	16,000 ft^2
Depth	11,085 ft
OOIP	550 MMBI
API Gravity	43°
Patterns	160
Spacing	80 acres
Permeability	20 mD
Porosity	15%
Project Duration	30 years
Oil Price	$75/bbl

The field consists of 160 patterns, and the total storage volume available in the reservoir using the parameters listed in **Table 14** is 4.27 x 10^9 ft^3. A storage efficiency factor (pore space utilization) of 45% was applied (the ratio of the total volume of purchased (i.e. stored CO_2) over the total available pore volume in the study area. This yields a total stored value of 793 Bcf over the study area – approximately 5 BCF per pattern.

CO_2 Prophet models yield incremental oil production ranging from 80 MMbbls (15% of OOIP) to 123 MMbbls (23% of OOIP), depending upon recovery efficiency factors applying current CO_2-EOR technologies and "Next Generation" CO_2-EOR technologies in the study area (Kuuskraa et al 2013). A total of 793 Bcf of CO_2 is purchased and stored during this operation at the 23% recovery efficiency. At $75/bbl oil, the economics from the cost model suggest that the net cash flow for the Prophet EOR case is $28/ bbl.

5.0 References

1) ARI. 2013a. Commercial Scale CO_2 Injection and Optimization of Storage Capacity in the Southeastern United States: Geologic Characterization Report, Deliverable 2.1. DE-FE0010554. August 22, 2013.

2) ARI. 2013b. Commercial Scale CO_2 Injection and Optimization of Storage Capacity in the Southeastern United States: Geostatistical Analysis of Southeastern Sediments Deliverable 3.2. DE-FE0010554. August 22, 2013.

3) Azzolina, N. A., Nakles, D. V., Gorecki, C.D., Peck, W.D., Ayash, S.C., Melzer, S., Chatterjee, S. 2015. CO_2 storage associated with CO_2 enhanced oil recovery: A statistical analysis of historical operations, International Journal of Greenhouse Gas Control, Vol. 37, Elsevier, Amsterdam, pp. 384-397.

4) Bishop, C.M. 1995. Neural Networks for Pattern Recognition. Oxford University Press, Inc. New York, NY, USA

5) Cant, D.J., and Walker, R.G. 1978. Fluvial Processes and Facies Sequence in the Sandy Braided South Saskatchewan River, Canada, Sedimentology, v. 25, no. 5, p. 625-648, 1978.

6) Eaves, E. 1976. Citronelle Oil Field, Mobile County, Alabama, in M 24: North American Oil and Gas Fields. AAPG Special Volumes. Pp. 259-275.

7) Esposito, R. A., Pashin, J. C., Walsh, P. M. 2008. Citronelle Dome: A giant opportunity for multizone carbon storage and enhanced oil recovery in the Mississippi Interior Salt Basin of Alabama. Environmental Geosciences, v 15 n., June 2008, P. 53-62.

8) Godec, M. 2017. Potential for CO_2 Storage Cost Reductions with Greater Commercial Deployment. Carbon Capture, Utilization & Storage Conference. Chicago Illinois April 10-15, 2017.

9) Hill, B., Hovorka, S., Melzer, S. 2013. Geologic carbon storage through enhanced oil recovery, Energy Procedia, Vol. 37, pp. 6808-6830.

10) Hopefield, J.J. 1982. Neural networks and physical systems with emergent collective computational abilities. Proceedings of the National Academy of Sciences of the United States of America. Volume 79, 8. Pp2554-2558.

11) IEA. 2015. Storing CO_2 through Enhanced Oil Recovery Combining EOR with CO_2 storage (EOR+) for profit. Online: <https://www.iea.org/publications/insights/insightpublications/Storing_CO_2_through_Enhanced_Oil_Recovery.pdf>

12) Jonsson, H., Cyphers, S., Petrusak, R., Koperna, G. 2013. Constructing a Reservoir Model to Simulate Commercial Scale CO_2 Injection and Optimization of Storage Capacity in the Southeastern United States. Carbon Management Technology Conference, CMTC 2013, Alexandria, Virginia, October 21-23, 2013.

13) Koperna, G.J., Riestenberg, D., Kuuskraa, V., Rhudy, R., Trautz, R., Hill, G., Esposito, R. 2012. The SECARB Anthropogenic Test: A US Integrated CO_2 Capture, Transportation and Storage Test. International Journal of Clean Coal and Energy, 2012, 1, 13-26

14) Koperna, G., Riestenberg, D., Petrusak, R., Esposito R., and Rhudy, R. 2009. Lessons Learned while Conducting Drilling and CO_2 Injection Operations at the Victor J. Daniel Power Plant in Mississippi, 2009 SPE Annual Technical Conference and Exhibition, New Orleans, 4-7 October 2009.

15) Koperna, G.J., Kuuskraa, V., Riestenberg, D., Rhudy, R., Trautz, R., Hill, G., Esposito, R. 2013. The SECARB Anthropogenic Test: Status from the Field. Energy Procedia, Volume 37, 2013, pp. 6273-6286.

16) Kovscek, A. R. and Cakici, M. D. 2005. Geologic storage of carbon dioxide and enhanced oil recovery. II. Co-optimization of storage and recovery, Energy Conversion and Management Vol. 46, pp 1941-1956.

17) Kuuskraa, V., and Wallace, M. 2014. CO_2-EOR set for growth as new CO_2 supplies emerge. Oil and Gas Journal Vol. 112, No. 4, pp. 66-77.

18) MacGregor, J.R., Petrusak, R., Cyphers, S.R., Jonsson, H., Oudinot, A., and Koperna, G.J. 2014. Constructing a Geologic Model to Simulate and Optimize Commercial Scale Injection and Storage of CO_2 at Citronelle Field, Mobile County, Alabama. AAPG Annual Convention and Exhibition, Houston, Texas, USA, April 6–9, 2014

19) Mancini, E. A., and Puckett, T. M. 2002. Transgressive-Regressive Cycles in Lower Cretaceous Strata, Mississippi Interior Salt Basin Area of the Northeastern Gulf of Mexico, USA, Cretaceous Research, v. 23, p. 409-438, 2002.

20) Miall, A. D. 1977. A Review of the Braided-River Depositional Environment, Earth-Science Reviews 13, 62 p, 1977.

21) Miall, A.D. 1978. Lithofacies Types and Vertical Profile Models in Braided River Deposits: A Summary in A.D. Miall, ed., Fluvial sedimentology, Canadian Society of Petroleum Geologists, Memoir 5, p. 597-604, 1978.

22) Mohaghegh, S. 2000. Virtual-Intelligence Applications in Petroleum Engineering: Part 1—Artificial Neural Networks. Journal of Petroleum Geology. Volume 52, Issue 9. September 2000.

23) Pashin, J. C., and Guohai Jin. 2004. Geometry and Evolution of Mesozoic-Cenozoic Salt Structures in the DeSoto Canyon and Eastern Mississippi Interior Salt Basins: Final Report, U.S. Minerals Management Service, Order 0101PO18256, 191 p., 2004.

24) Pashin, J. C., Kopaska-Merkel, D. C., and Hills, D. J. 2014. Reservoir Geology of the Donovan Sandstone in Citronelle Field, in Walsh, P. M., ed., Carbon Dioxide-Enhanced Oil Production from the Citronelle Oil Field in the Rodessa Formation, South Alabama: Final Scientific/Technical Report, U.S. Department of Energy Award DE-FC26-06-NT43029, p. 13-65, 2014.

25) Pashin, J.C., McIntyre, M.R., Grace, R.L.B. and Hills, D. J. 2008. Southeastern Regional Carbon Sequestration Partnership (SECARB) Phase IIII Final Report. September 30, 2008.

26) Petrusak, R. L., Goad, P. G., Koperna, G. J., and Riestenberg, D. E. 2009. FY2008 Annual Report Geologic Characterization Task Southeast Regional Carbon Sequestration Partnership (SECARB) on Geologic Characterization of the Lower Tuscaloosa Formation for the Phase II Saline Reservoir Injection Pilot Test, Jackson County, Mississippi, 2009.

27) Rust, B.R. 1977. Depositional Models for Braided Alluvium, in A.D. Miall, ed., Fluvial Sedimentology, Canadian Society of Petroleum Geologists, Memoir 5, p. 605-625, 1977.

28) UIC Permit. 2011. Alabama Department of Environmental Management UIC Permit, ALSI9949665. Class V Experimental well for the SECARB PHASE III ANTHROPOGENIC TEST. Denbury Onshore, LLC. Injection Well No. 2 (D-9-9#2) Mobile County, Alabama Citronelle Oil Field.

29) Wong, R., Goehner, A., McCulloch, M. 2013. Net Greenhouse Gas Impact of Storing CO_2 through Enhanced Oil Recovery (EOR), Pembina Institute, Calgary.

Appendix A: Reservoir Simulation Results

Table A.1: Commercial Scale CO_2 Injection and Optimization of Storage Capacity in the Southeastern United States: Results of Simulations using ARI's Upscaled Geologic Model, implemented in CMG/GEM, for Injection into Single and Stacked Formations in Citronelle Field having Low Heterogeneity.[1]

Formation	Volume of CO_2 Injected[2] (ft^3)	Layers Containing CO_2	Dimensions of Bounding Box[3] (ft)	Volume Bounded (ft^3)	Volume of Pore Space (ft^3)	Volume of Pore Space Containing CO_2 (ft^3)	Efficiency Pore Space Utilization (%)
Injection into Single Formations							
Upper Paluxy	5.840×10^{11}	275-336	10,000 x 10,500	7.354×10^{10}	1.060×10^{10}	1.847×10^{9}	17.42
Washita	5.840×10^{11}	150-209	10,000 x 9,000	8.664×10^{10}	1.507×10^{10}	2.213×10^{9}	14.69
Lower Tuscaloosa	5.840×10^{11}	120-149	17,500 x 18,000	8.779×10^{10}	1.843×10^{10}	2.448×10^{9}	13.28
Wilcox	6.77×10^{10}	5-13	7,500 x 6,500	1.006×10^{11}	2.213×10^{10}	1.623×10^{9}	7.33
Sequential Injection into Two Formations: Upper Paluxy – Washita							
Upper Paluxy	5.840×10^{11}	275-336	13,000 x 13,000	1.176×10^{11}	1.694×10^{10}	1.926×10^{9}	11.37
Washita	5.840×10^{11}	150-209	10,000 x 9,000	8.664×10^{10}	1.507×10^{10}	2.213×10^{9}	14.69
Sequential Injection into Two Formations: Upper Paluxy – Lower Tuscaloosa							
Upper Paluxy	5.840×10^{11}	275-336	13,000 x 13,000	1.176×10^{11}	1.694×10^{10}	1.926×10^{9}	11.36
Lower Tuscaloosa	5.840×10^{11}	120-149	17,500 x 18,000	8.779×10^{10}	1.843×10^{10}	2.448×10^{9}	13.28
Sequential Injection into Two Formations: Upper Paluxy – Wilcox							
Upper Paluxy	5.840×10^{11}	275-336	13,000 x 13,000	1.176×10^{11}	1.694×10^{10}	1.925×10^{9}	11.36
Wilcox	6.77×10^{10}	5-13	7,500 x 6,500	1.006×10^{11}	2.213×10^{10}	1.605×10^{9}	7.25

Table A.1: (Low Heterogeneity, continued)

Formation	Volume of CO_2 Injected[2] (ft^3)	Layers Containing CO_2	Dimensions of Bounding Box[3] (ft)	Volume Bounded (ft^3)	Volume of Pore Space (ft^3)	Volume of Pore Space Containing CO_2 (ft^3)	Efficiency of Pore Space Utilization (%)
Sequential Injection into Four Formations: Upper Paluxy – Washita – Lower Tuscaloosa – Wilcox							
Upper Paluxy	5.840×10^{11}	275-336	15,500 x 16,000	1.701×10^{11}	2.451×10^{10}	1.930×10^{9}	7.88
Washita	5.840×10^{11}	150-209	14,500 x 14,500	2.049×10^{11}	3.576×10^{10}	2.333×10^{9}	6.52
Lower Tuscaloosa	5.840×10^{11}	120-149	19,500 x 20,500	1.121×10^{11}	2.356×10^{10}	2.468×10^{9}	10.48
Wilcox	6.77×10^{10}	5-13	7,000 x 6,500	9.390×10^{10}	2.065×10^{10}	1.552×10^{9}	7.51

Notes
1. Model runs and post-processing by Gregory C. Myers, UAB.
2. Volume at surface conditions.
3. *x* x *y*, (West to East) x (South to North).

Table A.2: Commercial Scale CO_2 Injection and Optimization of Storage Capacity in the Southeastern United States: Results of Simulations using ARI's Upscaled Geologic Model, Implemented in CMG/GEM, for Injection into Single and Stacked Formations in Citronelle Field having High Heterogeneity.[1]

Formation	Volume of CO_2 Injected[2] (ft^3)	Layers Containing CO_2	Dimensions of Bounding Box[3] (ft)	Volume Bounded (ft^3)	Volume of Pore Space (ft^3)	Volume of Pore Space Containing CO_2 (ft^3)	Efficiency of Pore Space Utilization (%)
Injection into Single Formations							
Upper Paluxy	5.840×10^{11}	275-335	10,500 x 11,500	8.185×10^{10}	1.189×10^{10}	1.865×10^{9}	15.68
Washita	5.840×10^{11}	150-209	10,000 x 8,500	8.175×10^{10}	1.423×10^{10}	2.227×10^{9}	15.65
Lower Tuscaloosa	5.840×10^{11}	120-149	17,500 x 19,000	9.282×10^{10}	1.945×10^{10}	2.449×10^{9}	12.59
Wilcox	6.77×10^{10}	5-13	7,500 x 6,500	1.006×10^{11}	2.213×10^{10}	1.623×10^{9}	7.33
Sequential Injection into Two Formations: Upper Paluxy – Washita							
Upper Paluxy	5.840×10^{11}	275-335	13,500 x 13,000	1.181×10^{11}	1.707×10^{10}	1.924×10^{9}	11.27
Washita	5.840×10^{11}	150-209	10,000 x 8,500	8.175×10^{10}	1.423×10^{10}	2.226×10^{9}	15.64
Sequential Injection into Two Formations: Upper Paluxy – Lower Tuscaloosa							
Upper Paluxy	5.840×10^{11}	275-335	13,500 x 13,000	1.181×10^{11}	1.707×10^{10}	1.924×10^{9}	11.27
Lower Tuscaloosa	5.840×10^{11}	120-149	17,500 x 19,000	9.282×10^{10}	1.945×10^{10}	2.449×10^{9}	12.59
Sequential Injection into Two Formations: Upper Paluxy – Wilcox							
Upper Paluxy	5.840×10^{11}	275-335	13,500 x 13,000	1.181×10^{11}	1.707×10^{10}	1.923×10^{9}	11.27
Wilcox	6.77×10^{10}	5-13	7,500 x 6,500	1.006×10^{11}	2.213×10^{10}	1.618×10^{9}	7.31

Table A.2: (High Heterogeneity, continued)

Formation	Volume of CO_2 Injected[2] (ft^3)	Layers Containing CO_2	Dimensions of Bounding Box[3] (ft)	Volume Bounded (ft^3)	Volume of Pore Space (ft^3)	Volume of Pore Space Containing CO_2 (ft^3)	Efficiency of Pore Space Utilization (%)
Sequential Injection into Four Formations: Upper Paluxy – Washita – Lower Tuscaloosa – Wilcox							
Upper Paluxy	5.840×10^{11}	275-335	17,000 x 17,500	1.956×10^{11}	2.821×10^{10}	1.929×10^{9}	6.84
Washita	5.840×10^{11}	150-209	15,000 x 13,500	1.970×10^{11}	3.422×10^{10}	2.332×10^{9}	6.81
Lower Tuscaloosa	5.840×10^{11}	120-149	19,000 x 21,000	1.120×10^{11}	2.344×10^{10}	2.469×10^{9}	10.53
Wilcox	6.77×10^{10}	5-13	7,500 x 6,500	1.006×10^{11}	2.213×10^{10}	1.612×10^{9}	7.29

Notes
1. Model runs and post-processing by Gregory C. Myers, UAB.
2. Volume at surface conditions.
3. *x* x *y*, (West to East) x (South to North).

Appendix B: Measurements of Permeability and Minimum Capillary Displacement Pressure

B.1 Introduction

An important component of the Commercial Scale project was to assess the permeability and minimum capillary displacement pressure of core samples collected from the wells drilled for the SECARB Anthropogenic Test site. These measurements provide data integral to better constrain the petrophysical parameters of the study area and enhance the modeling output. Minimum capillary displacement pressure and effective permeability are the experimental results of the method developed by A. Hildenbrand and coworkers at RWTH Aachen University (Hildenbrand et al., 2002, 2004), for quantitative assessment of the potential for seepage of gas through brine-saturated fine-grained rocks. The "minimum capillary displacement" pressure measurement is an alternative to the traditional method of increasing the pressure of gas on one face of a brine-saturated plug in small increments, until breakthrough is observed. The traditional method tends to overestimate the breakthrough pressure, because there can be a lag time of days or weeks before gas appears on the downstream side of a plug, even at upstream pressures well above the pressure ultimately identified as the true breakthrough pressure.

The single-phase permeabilities were 2.95 ± 0.03 microdarcy (CO_2 gas) and 2 ± 1 nanodarcy (N_2 gas) for plugs from Cores 2FD and 3FD, respectively. The minimum capillary displacement pressure, at which breakthrough is just possible given sufficient time, was determined using N_2 on brine-saturated plugs. The minimum capillary displacement pressures were 1.2 MPa (174 psi, NaCl brine) and 4.31 MPa (625 psi, KCl brine) for plugs from Cores 2FD and 3FD, respectively.

B.2 Methodology

Measurements of permeability to gas, minimum capillary displacement pressure, and effective permeability to gas in the presence of brine were made on sample plugs cut, perpendicular to bedding, from core samples 2FD and 3FD from Well D-9-9 No. 2 at Citronelle at depths near 9,400 ft. The plug from Core 3FD, however, broke up while submerged in brine under vacuum, in preparation for determination of the minimum capillary displacement pressure (following permeability analysis). A second plug was cut from the long 1-inch-diameter plug shown in **Figure B.1**, just below the location from which Plug 3FD-1 had been taken. The practice of submerging the plugs in brine under vacuum, to saturate them, was discontinued. Properties of the plugs and conditions of the measurements of minimum capillary displacement pressure and effective permeability are summarized in **Table B.1 and Table B.2**.

To assess permeability, a sample was first saturated with brine, after mounting in the core holder, by filling the cavity above the sample, which becomes the downstream volume during the measurements, with brine, and applying a steady, regulated high pressure of nitrogen until brine

flowed out from the other end of the plug. Nitrogen at constant pressure, above the anticipated breakthrough pressure, was then applied to the upstream (lower) end of the plug, with the downstream (upper) end at atmospheric pressure, and the valve on the downstream side was closed, sealing the cavity on that end. As gas flows through the sample, the difference in pressure, upstream to downstream, asymptotically approaches a residual pressure difference corresponding to the capillary pressure in the narrowest throat in the highest conductivity pore connecting the upstream and downstream faces of the sample.

Determination of the minimum capillary displacement pressure begins with a plug completely saturated with brine (100% brine saturation, where its permeability to gas is zero) and an initial pressure difference across the sample greater than the anticipated breakthrough pressure. During the decay of the pressure to equilibrium, the gas phase saturation first increases as pores are drained, then decreases as brine is reimbibed, as the pressure approaches its final residual value. At the point where the process reverses, from drainage to imbibition, the effective permeability passes through a maximum. The data were analyzed to determine the dependence of the effective permeability on the pressure difference across the sample. The effective permeability to gas during the decay in pressure drop and evolution of brine and gas saturations was found to depend on the 4th power of the difference between the excess pressure on the upstream face of the plug and the excess pressure at the maximum effective permeability. This provides a correlation with which the rate of seepage through a confining layer can be anticipated as a function of the pressure exerted by a layer of CO_2 trapped beneath it, for columns of CO_2 above the critical height for breakthrough.

Figure B.1: Four-Inch Diameter Cores 2FD and 3FD from Well D-9-9 No. 2 in the Citronelle Field

Table B.1: Properties of Sample Plugs and Conditions During Measurement of Permeability

Property	Sample Plug 2FD-1	Sample Plug 3FD-1
Origin	Citronelle Field	Citronelle Field
Well	D-9-9 No. 2	D-9-9 No. 2
Depth at top of plug	9431.3 ft	9442.1 ft
Formation	Upper Paluxy	Upper Paluxy
Orientation	Perpendicular to bedding	Perpendicular to bedding
Diameter	0.02518 m	0.02461 m
Length	0.02680 m	0.02637 m
Fluid	CO_2	N_2
Temperature	19.8 - 20.7 °C	21.3 - 21.6 °C
Upstream Pressure	110 - 336 psig	1006 - 2525 psig
Axial and Radial Overburden Pressures	1200 psig	3000 psig
Permeability	2.95 ± 0.03 microdarcy	2 ± 1 nanodarcy

Table B.2: Properties of Sample Plugs and Conditions During the Measurements of Minimum Capillary Displacement Pressure and Effective Permeability

Property	Sample Plug 2FD-1	Sample Plug 3FD-2
Origin	Citronelle Field	Citronelle Field
Well	D-9-9 No. 2	D-9-9 No. 2
Depth at top of plug	9431.3 ft	9442.2 ft
Formation	Upper Paluxy	Upper Paluxy
Orientation	Perpendicular to bedding	Perpendicular to bedding
Diameter	0.02518 m	0.02462 m
Length	0.02680 m	0.029275 m
Non-Wetting Fluid	N_2	N_2
Wetting Fluid	Brine (10 g NaCl/L)	Brine (100 g KCl/L)
Temperature	21.0 - 22.3 °C	19.9 - 23.1 °C
Upstream Pressure	815 - 820 psig	2780 - 2910 psig
Axial and Radial Overburden Pressures	1200 psig	4000 psig
Minimum Capillary Displacement Pressure, P_d	1.2 MPa 174 psi	4.31 MPa 625 psi
Maximum Effective Permeability, $k_{eff,max}$	0.092 microdarcy	6.7 nanodarcy
Excess Pressure at Maximum Effective Permeabilty, P_{max}	3.55 MPa 515 psi	11.9 MPa 1726 psi

B.3 CO_2 Leakage through a Confining Layer in the Absence of Chemical Reactions

Assessment of CO_2 leakage through a confining layer in the absence of chemical reactions was conducted on a core sample plug applying the underground gas storage model of Hildenbrand, Schlömer, Krooss, and Litke (2004). The model, which includes breakthrough and leakage through confining layers, was augmented by applying the equation relating effective permeability and pressure to leakage of CO_2 by capillary flow through a seal. The result is a simple model describing the breakthrough and history of CO_2 leakage through a confining layer, including the effects of changes in the height of CO_2 column due to loss of CO_2 and continued CO_2 injection, should breakthrough not be detected by the operators of a sequestration project. A relationship between the effective permeability to gas and pressure drop across a core sample plug was determined by measurements of gas flow through a sample during drainage and imbibition of brine by the sample with change in pressure.

There are four adjustable parameters in the equation for the effective permeability, determined in the laboratory by experiment: 1) the minimum capillary displacement pressure, 2) maximum effective permeability, 3) the pressure at the maximum permeability, and 4) the exponent of the dimensionless pressure difference. The maximum effective permeability occurs at the minimum brine saturation and maximum gas saturation reached under the conditions in the confining layer.

Stored CO_2 is treated as forming an approximately uniform layer with constant depth, provided dispersion of injected CO_2 is sufficiently rapid to combine any plumes from neighboring wells. Calculations of CO_2 storage under a seal at a depth of 9430 ft were conducted utilizing the following parameters: 1) a minimum capillary displacement pressure of 1.2 MPa (174 psi); 2) a maximum effective permeability of 0.095 microdarcy; 3) pressure at maximum permeability of 3.55 MPa (515 psi); and 4) CO_2 injection rate of 500 metric tons/day into wells on 40-acre centers, in a reservoir having porosity of 19%. **Table B.3** details all the parameters chosen for modeling.

Under the conditions modeled, the minimum capillary displacement pressure was exceeded, leading to breakthrough after 29 years. The CO_2 retention of confining layers with thicknesses ranging from 1 to 100 meters was examined following injection operations lasting from 40 to 55 years. The assessment period for containment ranged from 100 to 1000 years. At 100 years, more than 99% of injected CO_2 was retained under confining layers with thicknesses of 5 m or greater (**Figure B.2**). To retain 99% of injected CO_2 for 1000 years, a seal more than 50 m thick was required (**Figure B.3**). Extension of the injection period from 40 years to 45, 50, and 55 years yielded a limited sensitivity of CO_2 retention, where minimal loss was observed (**Figure B.4**).

How does this compare to the modeling results from the previous section?

Table B.3: Conditions Selected to Assess CO_2 Leakage for the Reservoir and Confining Layer

Conditions Chosen for the Reservoir and Confining Layer.*	
CO_2 injection rate	3.575×10^{-5} kg/(m^2·s) †
Injection period	40, 45, 50, and 55 years
Porosity of reservoir	0.19
Time to breakthrough	28.9 years
Critical CO_2 column height, at breakthrough	273 m
Depth at the interface between the reservoir and confining layer, x_1	2875 m
Thickness of the confining layer, $x_1 - x_2$	1, 2, 5, 10, 20, 50, and 100 m
Temperature, T	383.15 K (230 °F)
Density of CO_2, ρ_{CO_2}	626.2 kg/m^3 ‡
Density of brine, ρ_{brine}	1075.6 kg/m^3 §
Absolute viscosity of CO_2, μ	5.056×10^{-5} Pa·s ‡
Minimum capillary displacement pressure, P_d	1.2 MPa
Maximum effective permeability, $k_{eff,max}$	9.38×10^{-20} m^2 0.095 microdarcy
Excess pressure at maximum permeability, P_{max}	3.55 MPa
Exponent, n, of the dimensionless pressure difference in Equation (5)	3

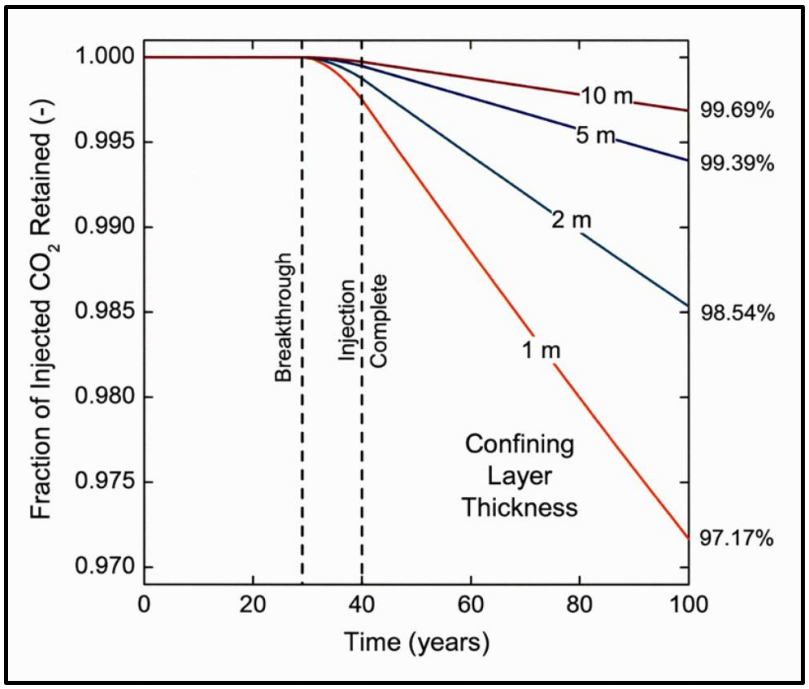

Figure B.2: Fractions of CO_2 Remaining Trapped Under Confining Layers having Thicknesses Of 1, 2, 5 and 10 M, after 100 Years, following Injection of CO_2 at the Rate of 500 Metric Tons/Day into Wells on 40-Acre Centers for 40 Years. Breakthrough of CO_2 Occurs at Approximately 29 Years, at Least 11 Years Earlier than Expected in the Design of the Project, and goes Undetected, so Injection Continues to the Planned 40 Years.

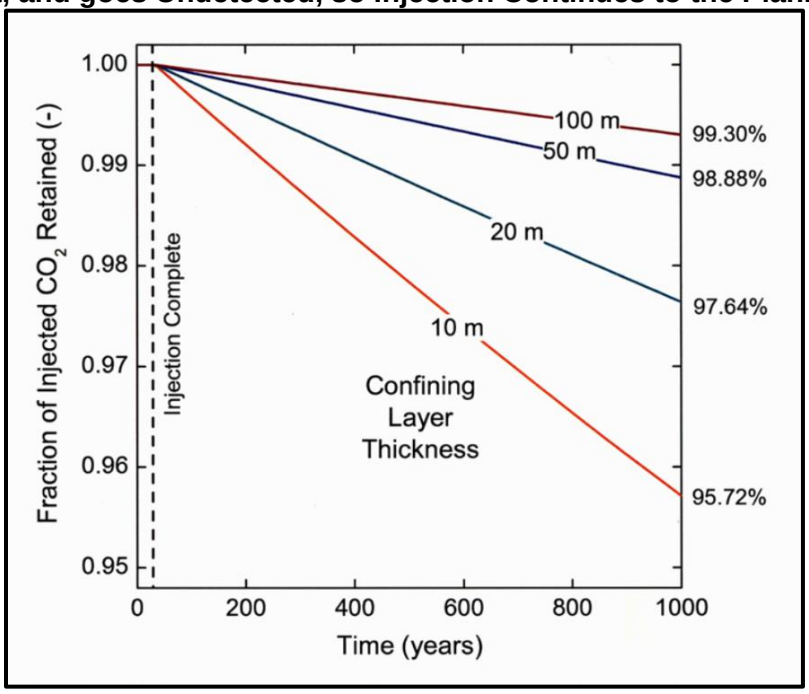

Figure B.3: Fractions of CO_2 remaining trapped under confining layers having thicknesses of 10, 20, 50, and 100 m, after 1000 years, following injection of CO_2 at the rate of 500 metric tons/day into wells on 40-acre centers for 40 years. Breakthrough of CO_2 occurs at approximately 29 years, as in Figure 3, but injection continues to the planned 40 years.

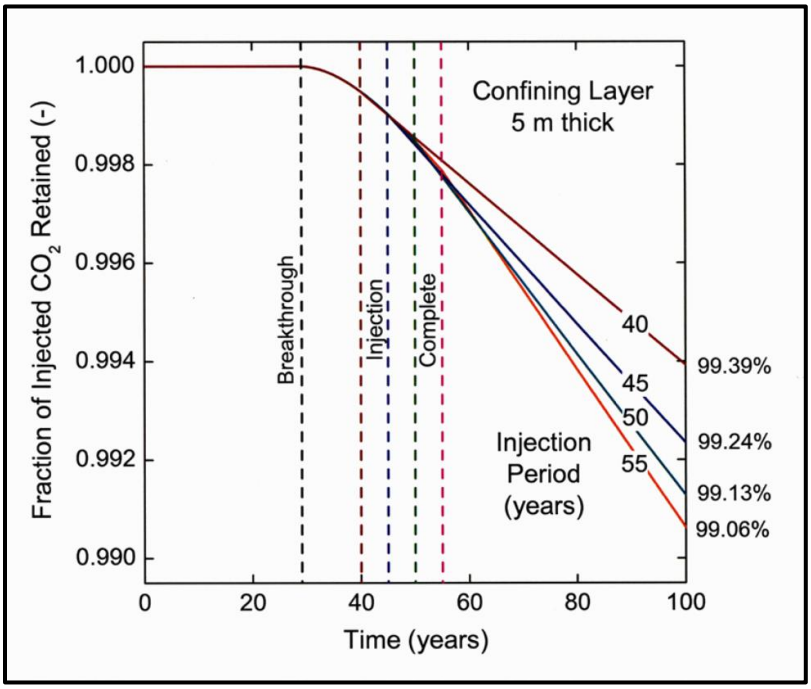

Figure B.4: Fractions of CO_2 remaining trapped under a confining layer 5 m thick after 100 years, following injection of CO_2 at the rate of 500 metric tons/day into wells on 40-acre centers for periods of 40, 45, 50, and 55 years, with CO_2 breakthrough occurring, as in Figures 3 and 4, at approximately 29 years.

B.4 Changes in the Permeability for a Barrier Layer Exposed to CO_2 and Brine

Simulations using the TOUGHREACT-ECO_2N simulator from Lawrence Berkeley National Laboratory were performed to evaluate CO_2 migration and CO_2-mineral reactions during and following CO_2 injection into the Upper Paluxy formation in the Citronelle Field.

The model employed a two-dimensional symmetric radial grid divided vertically into nine layers. The bottom four layers were allocated to the sandstone reservoir section and the upper five layers were assigned to the shale caprock formation above the reservoir. A single injection well was placed at the center of the radial grid, injecting 10 million ft^3/day of CO_2 into each of the four sandstone layers. CO_2 injection at this rate continued for 40 years, followed by a shut-in period of 9,960 years. The grid extended outward, to a distance of 100,000m (328,084 ft) from the injection well, to ensure that the simulation was able to maintain a constant pressure at the boundary, acting as an infinite reservoir.

The diameter of the injection well was 0.14 m (5.5 in), and the grid block length in the radial direction was increased progressively, with increasing distance from the well-bore, according to a logarithmic rule implemented by the simulator internally. The progressive increase in grid block

length provided sufficient resolution of the injection process in the high pressure region near the well bore, while maintaining constant pressure at the outer boundary. Values of the model input parameters are specified for each layer in **Table B.4**.

To simulate chemical processes, TOUGHREACT-ECO$_2$N requires, as inputs, the initial volume fractions of the formation's primary mineral components and their reaction kinetic parameters. Minerals that precipitate during and after CO_2 injection are classified as secondary and their formation depends upon the primary minerals considered. The primary minerals and their abundances (volume %) were: quartz, 22.1; illite, 14.7; smectite, 6.0; kaolinite, 5.8; oligoclase, 3.4; hematite 2.1; and chlorite, 1.7.

Dolomite was intentionally excluded because of the wide variation in its abundance in the formation and because of its great influence on the mineralization of CO_2. The simulation results presented here therefore provide a baseline minimum estimate of mineralized CO_2 yields that could be reached in Upper Paluxy sandstone. A separate simulation that included 40 vol% dolomite was also performed and the resulting yields of mineralized CO_2 were significantly higher.

The percent by volume distribution of primary minerals was the same in the sandstone and caprock layers. This assumption was based on the similarity of the composition matrices for the caprock and sandstone formations. Differentiation between sandstone and caprock properties was based only on their permeability, porosity, and compressibility.

The output parameters of greatest interest were CO_2 migration and CO_2 mineralization (i.e. CO_2 permanently sequestered). The results are presented in **Figures B.5** and **B.6**. As shown in **Figure B.6**, the distribution of gas phase CO_2 during the 40-year injection period is contained primarily within the sandstone layers, with very little penetration into caprock layers. It can also be noted in Figure 1 that, during the injection period, the gas phase CO_2 distribution over the thickness of the sandstone layers gradually develops the expected profile driven by buoyancy forces acting on the gas phase CO_2.

Table B.4: Upper Paluxy TOUGHREACT-ECO$_2$N Multi-Layer Model Inputs

Layer	**Legend** CR = caprock SS = sandstone	**Thickness layer** m (ft)	**Pressure at center of grid block** MPa (psi)	**Temperature at center of grid block** °C (°F)	**Permeability (isotropic)** millidarcy	**Porosity (isotropic)** %	**CO_2 injection rate** kg/s (ft^3/day)
1	CR1	9.75361 (32.0)	276.15 (4005.2)	80.3 (176.5)	9.7	9.5	0
2	CR2	9.75361 (32.0)	277.10 (4019.0)	81.3 (178.3)	9.7	9.5	0
3	CR3	9.75361 (32.0)	278.06 (4033.0)	82.3 (180.1)	9.7	9.5	0

4	CR4	9.75361 (32.0)	279.00 (4046.6)	83.3 (181.9)	9.7	9.5	0
5	CR5	9.75361 (32.0)	280.06 4061.9)	84.3 (183.7)	9.7	9.5	0
6	SS1	36.25 (118.9)	282.80 (4101.7)	86.3 (187.3)	19.3	16.3	6.2875 (10,000, 000)
7	SS2	36.25 (118.9)	287.60 (4171.3)	88.3 (190.9)	19.3	16.3	6.2875 (10,000, 000)
8	SS3	36.25 (118.9)	292.40 (4240.9)	90.3 (194.5)	19.3	16.3	6.2875 (10,000, 000)
9	SS4	36.25 (118.9)	297.16 (4309.9)	92.3 (198.1)	19.3	16.3	6.2875 (10,000, 000)

At 100 years, a small fraction of the gas phase CO_2 has penetrated the two lowest caprock layers, CR4 and CR5. Most of this CO_2 is in the very lowest caprock layer, CR5, adjacent to the sandstone reservoir, with only a tiny amount in the next higher layer, CR4. At 1,000 years, most of the CO_2 in the sandstone reservoir layers has accumulated in the top-most layer, SS1. Additional gas phase CO_2 has, however, migrated into caprock layers CR5 and CR4 with a tiny amount now appearing in higher caprock layers, CR3 and CR2. At 10,000 years 65% by mass of the gas phase CO_2 has migrated into the caprock layers while 35% remains in the sandstone layers. However, the fraction of CO_2 in the gas phase at 10,000 years is only 72% of the CO_2 mass in the gas phase at the end of the injection period. The remaining CO_2 is in solution with brine or has been permanently sequestered by mineralization.

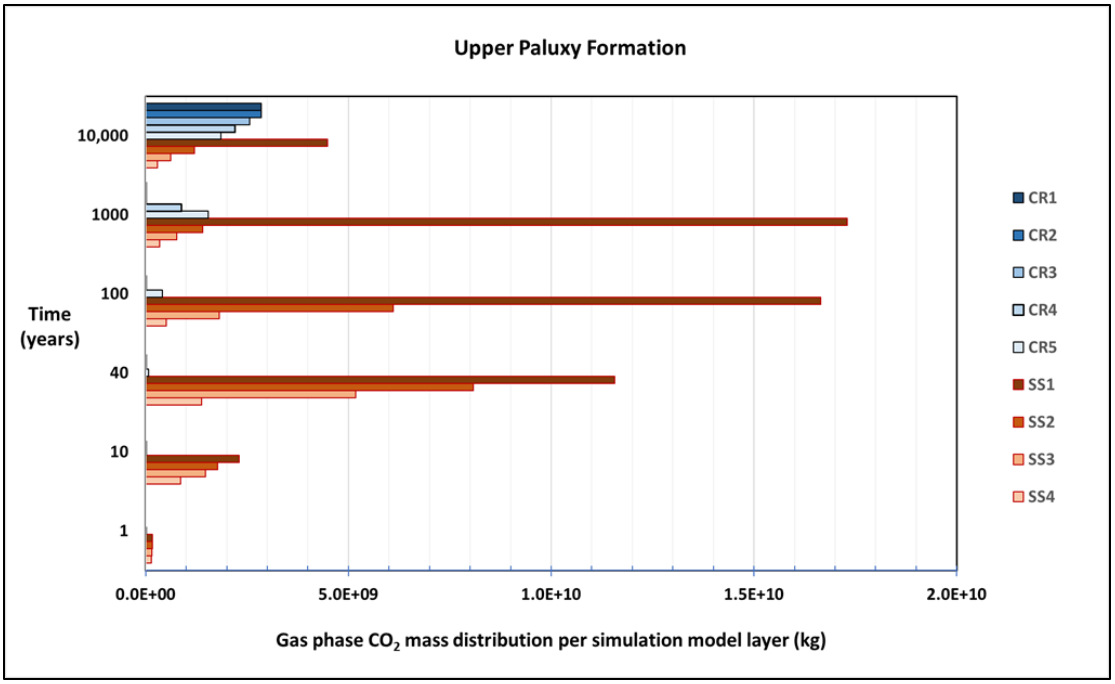

Figure B.5: Distribution of CO_2, by Mass, among the Sandstone Reservoir and Caprock Model Layers at 1, 10, 40, 100, 1,000 and 10,000 Years

The CO_2 mass per unit volume of formation permanently sequestered by chemical reactions with primary minerals is shown in **Figure B.6**. At 40 years, the amount of CO_2 mineralized averages 1.5 kg/m^3 of formation, with most of the chemical activity taking place in the transition zone where supercritical CO_2 and the liquid aqueous brine phases coexist, with partitioning and mixing between the two phases taking place continuously. At 1,000 years, the average yield of CO_2 permanently sequestered by mineralization increases to approximately 17 kg/m^3 of formation and takes place along the radial fringe of the CO_2 saturation profile. At 10,000 years the average yield of mineralized CO_2 reaches approximately 25 kg/m^3 of formation.

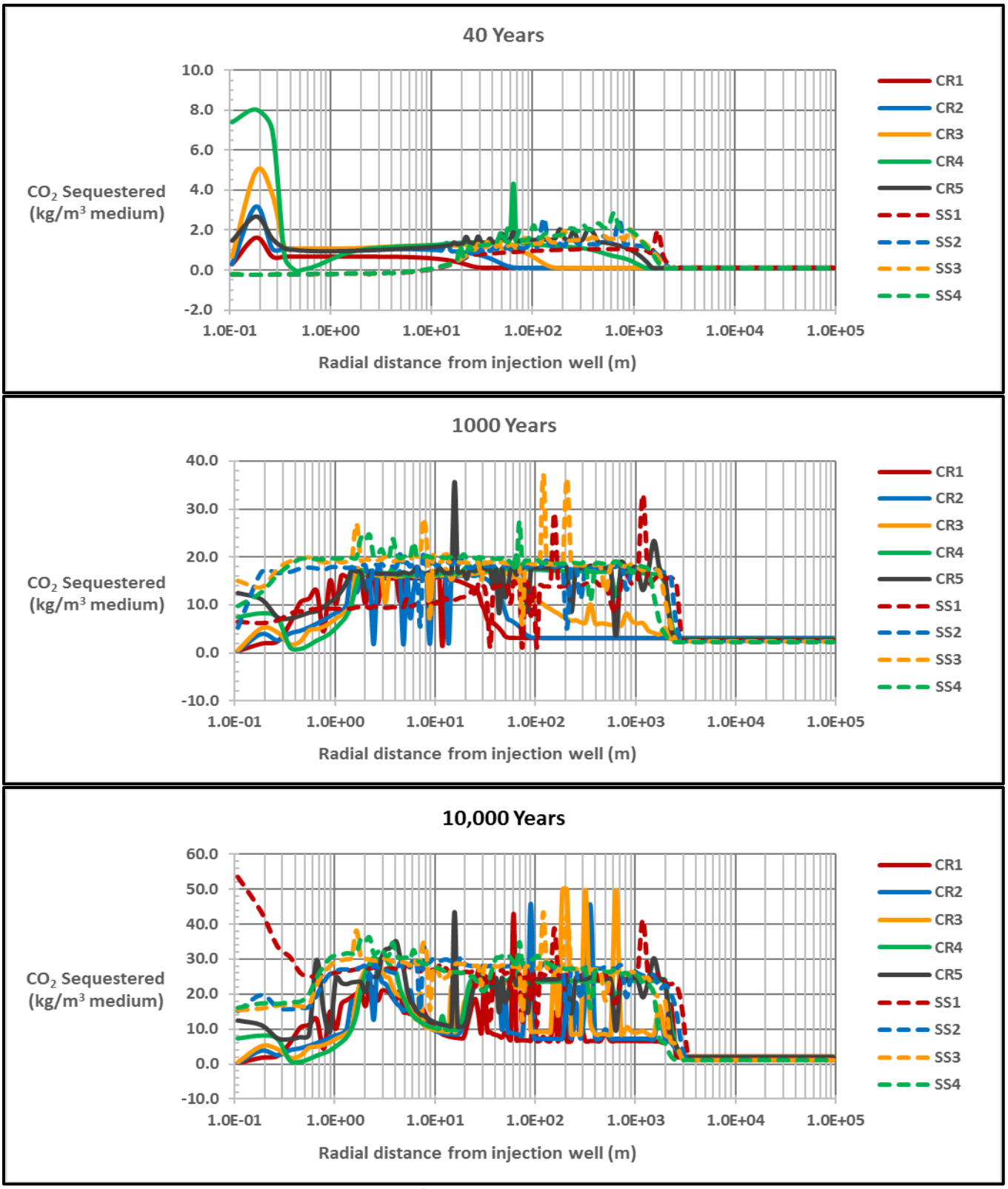

Figure B.6: Yields of CO_2 (Kg CO_2/M^3 of Formation) Permanently Sequestered by Mineralization in the Individual Sandstone Reservoir and Caprock Layers at 40, 1,000, and 10,000 Years

A sample of rock serving as a barrier layer to upward migration of CO_2 in the Paluxy Formation, at a depth of 9431 ft in the Citronelle Field, was exposed to flows of NaCl brine and a solution of CO_2 in NaCl brine for a total of 47 days. The permeability of the rock to CO_2 gas had been determined previously as 2.95 microdarcy and its minimum capillary displacement pressure (breakthrough pressure) as 1.2 MPa (174 psi), as reported in Deliverable 8.1. A photograph of the 4-inch diameter drill core and the 1 inch diameter sample plug cut from it, perpendicular to bedding, are shown in **Figure B.7**. The depth of Core 2FD is 9431.3 to 9431.8 ft. Sample No. 2FD-1 is the sample plug whose permeability was monitored during exposure to brine and solution of CO_2 in brine. The mineral analysis of the rock was (wt%): quartz, 20.9; K feldspar, 1.1; plagioclase, 3.2; calcite, 0.4; Fe dolomite, 43.2; siderite, 0.5; hematite, 3.9; and clays, 26.8. The composition of the clays was (wt% of the clays): illite/smectite, 21.2; illite and mica, 52.0; kaolinite, 20.1; and chlorite, 6.7.

The sample was mounted in a Core Lab/TEMCO triaxial core holder and placed in a laboratory oven at 70 ^{o}C. The brine and CO_2-brine solution were delivered to the upstream face of the sample from a Teledyne ISCO syringe pump at an average pressure of 8.4 MPa (1200 psig). The pressure at the downstream side of the sample was maintained at approximately 7.7 MPa (1100 psig) by adjustment of a metering valve. A photograph of the apparatus is shown in **Figure B.8**. The concentration of NaCl in the brine was 121.85 g NaCl/1000 g H_2O and the concentration of CO_2 in the CO_2-brine solution was 18.87 g CO_2/1000 g H_2O, equal to 80% of the CO_2 concentration in a saturated solution in the brine at the temperature of the sample and at the pressure at the outlet from the sample. The concentration of CO_2 was chosen to ensure that the CO_2 would remain in solution while passing through the sample and that only the liquid phase would be present in the sample.

A typical run consisted of measurements of the temperatures and pressures at the inlet and outlet from the sample and the time required for a volume increment of 0.08 mL of brine or solution of CO_2 in brine to flow through the sample, determined from the volume and time measurements indicated by the syringe pump. Roughly an hour was required for 0.08 mL of the brine or CO_2-brine solution to pass through the sample. The average and standard deviation of permeabilities determined from a sequence of five such runs was the usual procedure for establishing the condition of the sample on a given day.

The sample underwent a complex sequence of changes in permeability on exposure to the NaCl brine and the solution of CO_2 in the brine, as shown in **Figure B.9**. The sample was exposed only to brine for the first 20 days, then to the solution of CO_2 in brine for the next 27 days. When first exposed to the solution of CO_2 in brine, from day 20 to day 23, fine particles appeared in the CO_2-brine effluent from the sample and the solution became yellow, but only for those three days. Between the measurements on days 26 and 27 there was an upset when the confining pressure on the sample dropped unexpectedly. The exact effect of this event is unknown, but the upward trend in permeability following the incident had already been established before the upset occurred.

At the outset, after establishing the desired conditions of temperature, pressure, and flow of NaCl brine, the permeability of the sample decreased, over a period of ten days, from 0.93 to 0.83 microdarcy, then remained at 0.83 microdarcy for the next six days. The average permeability during this initial period, when the sample was exposed only to brine, was 0.874 ± 0.035 microdarcy. On the introduction of CO_2 to the brine, the permeability decreased further, over a period of three days, to 0.71 microdarcy, accompanied by the appearance of fine particles and a yellow color in the liquid effluent. The permeability then began to increase, and returned, over a period of four days, to 0.84 microdarcy. During the latter period, there was an upset in the confining pressure that briefly reversed the upward trend, but the upset condition is not thought to have altered the longer-term trend of increasing permeability that was already underway. The permeability then settled at an average value of 0.850 ± 0.021 microdarcy for the remaining 20 days of the test, all the while in the presence of the CO_2-brine solution. The net change, from the average permeability during the initial exposure to brine alone, to the average during the last 20 days of exposure to CO_2 and brine, was a reduction in permeability of only 3%.

The aspect of the observed evolution of permeability that seems most transparent is the reduction in permeability on introduction of CO_2 and the appearance of particles and yellow color in the effluent. Particles mobilized by dissolution of minerals but too large to pass through pore throats would have been responsible for the loss of permeability. The initial drop in permeability during the first 10 days of testing is not expected to have been due to mobilization of particles, because the NaCl concentration was thought to be sufficiently high to prevent release of particles from pore walls in the absence of CO_2.

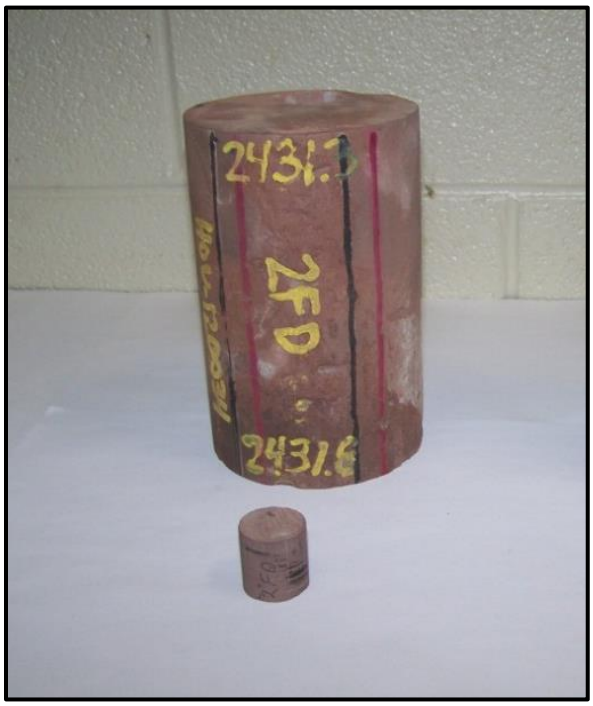

Figure B.7: Four-Inch Diameter Core 2FD from Well D-9-9 No. 2 in the Citronelle Field and the One-Inch Diameter Plug, Sample No. 2FD-1, Cut from it

Figure B.8: Set-Up of the Triaxial Core Holder and Syringe Pump for Measurement of Changes in Permeability of Plug 2FD-1 while Exposed to Nacl Brine and Solution of CO_2 in Brine

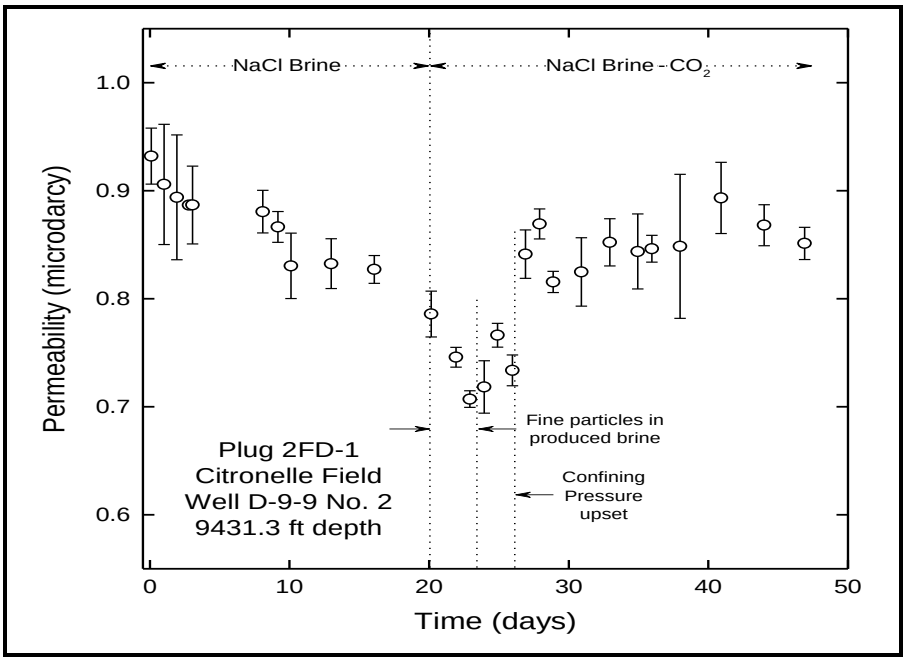

Figure B.9: Measurements of the Evolution of the Permeability of Sample Plug 2FD-1 During Exposure to Nacl Brine and a Solution of CO_2 in Nacl Brine

Appendix C: Paluxy Depositional Systems

C.1 Paluxy Litho-Stratigraphic Units and Sedimentology

The depositional setting of the sedimentary continuum of the Paluxy Formation at Citronelle Oil Field in southwest Alabama was assessed here to create a model of the depositional environment and infer modern analogues. Assessment of the depositional system provides insight to factors controlling CO_2 storage potential in reservoirs, and may constrain depositional reservoir characteristics amenable to store commercial quantities of anthropogenic CO_2. Core data and geophysical logs from three recently drilled wells in the Southeast Citronelle Oil Unit, in addition to petrographic and geo-chemical analyses of rock samples were utilized to conduct this assessment.

Petrographic analysis of cores and geophysical logs were applied to determine framework sandstone composition, sandstone diagenesis, and reservoir architecture. Results show that the sandstone units are predominantly arkosic. Porosity and permeability are well-developed in the sandstone especially in the Upper Paluxy, where average porosity and permeability values are 19 percent and 200 mD respectively. Intergranular pores predominate, and are common within feldspar grains. Quartz is the most abundant authigenic cement and primarily forms overgrowths; pore-filling calcite and ferroan dolomite are also common. Authigenic clay includes grain-coating illite and pore-filling kaolinite.

The average thickness of the Paluxy Formation is approximately 1,100 ft. centered on the Citronelle Dome. Core analyses indicate that the Paluxy represents a coarsening-upward succession composed of numerous stacked, aggradational sandstone-mudstone packages. Individual sandstone bodies have sharp bases, typically fine upward, and range in thickness from less than 10 ft. to more than 40 ft. Although some sandstone units have great lateral continuity, each well may have substantially different geophysical log signatures, reflecting internal reservoir heterogeneity among wells.

Sedimentologic analysis of the Paluxy Formation suggests a fluvial depositional environment that included bedload-dominated fluvial systems and interfluvial paleosols. The Paluxy Formation is a net coarsening-upward succession composed of numerous stacked, aggradational sandstone-mudstone packages. Individual sandstone bodies have sharp bases which typically fine upward, and range in thickness from less than 10 ft. to over 40 ft. Sedimentological analysis demonstrates that the Paluxy Formation was deposited in a continental environment that included bedload-dominated fluvial systems and interfluvial paleosols (**Figure C.1**). The braided channel complex and longitudinal bars of the Paluxy Formation are represented by the conglomerate facies and the sandstone facies. Cross-bedded sandstone represents braided channel complexes, while the deeply reddened and bioturbated sandstone bodies represent longitudinal bars.

The mudstone units separating the reservoir sandstone bodies are interpreted as interfluvial paleosols (**Figure C.2 and C.3**). These mudstone units are characterized by thick, clay-rich,

slicken sided mudstone, often with internal horizons of deformation, caliche glaebules, and caliche crack fills.

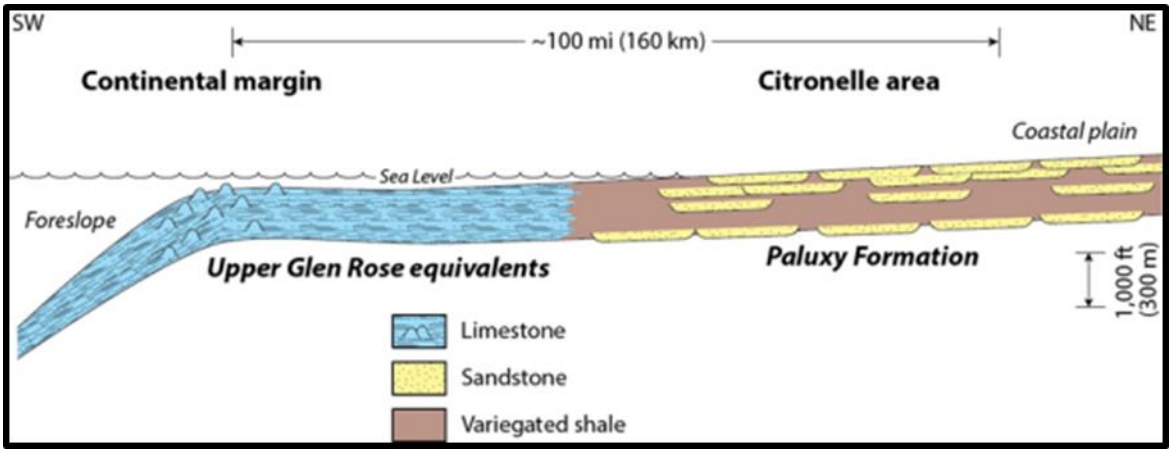

Figure C.1: Generalized Facies Diagram Showing Relationship of the Paluxy Formation to Equivalent Carbonate Deposits of the Gulf of Mexico Region (Modified from Pashin et al., 2014)

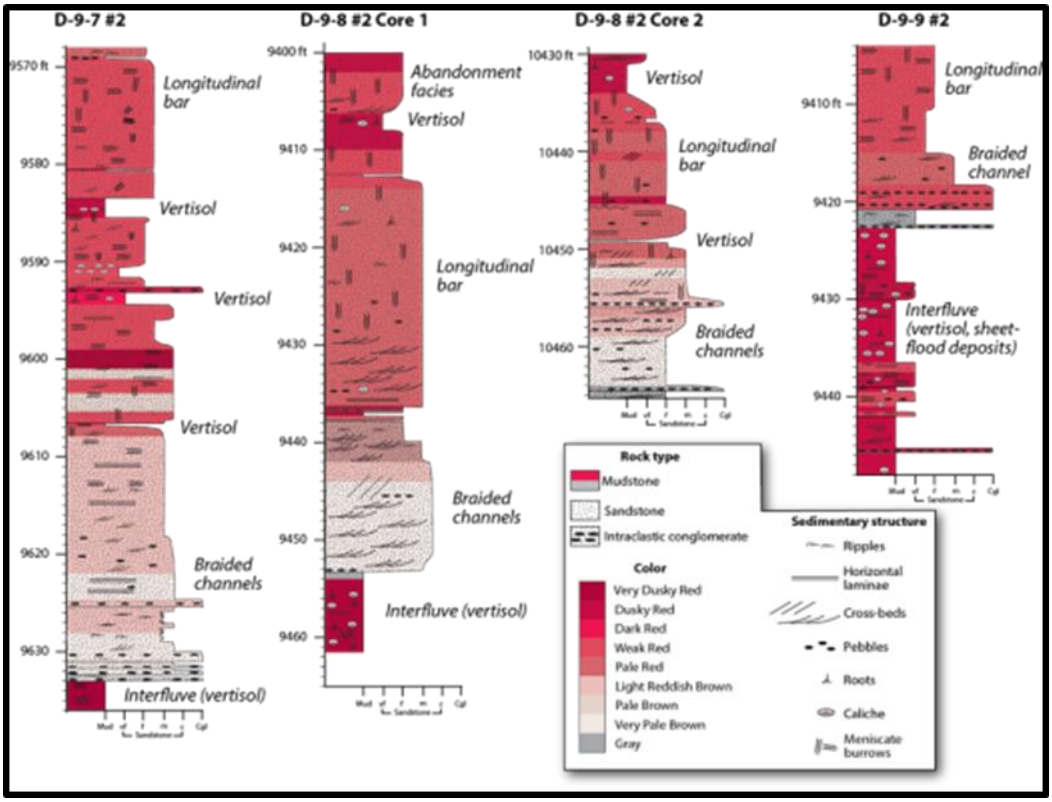

Figure C.2: Graphic Core Logs Showing Schematic Diagram of the Depositional Environment of the Paluxy Formation

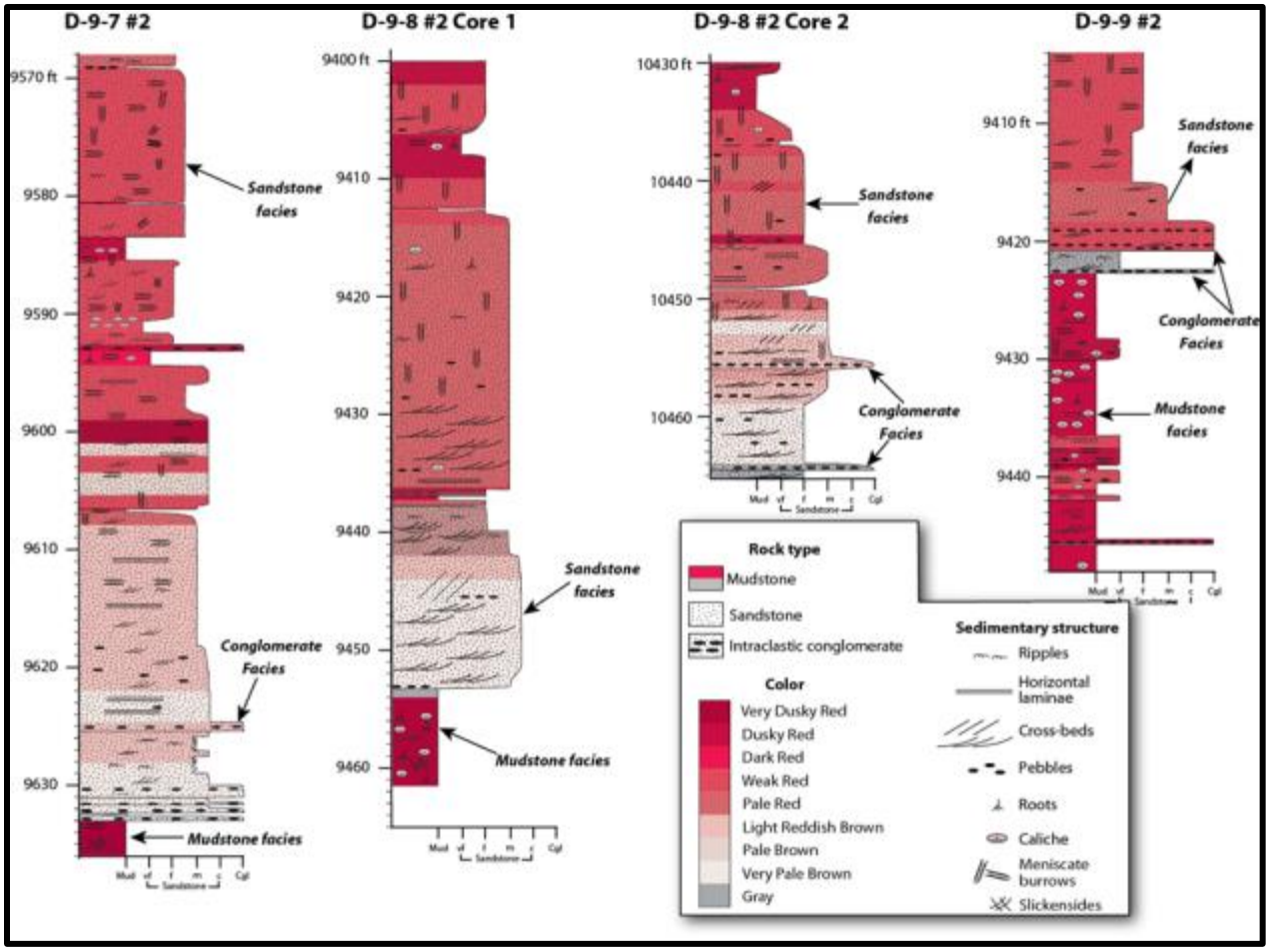

Figure C.3: Graphical Core Logs Showing Major Lithofacies, Rock Types, Color Variations, Sedimentary and Biogenic Structures, and Common Vertical Successions in the Paluxy Formation

The Paluxy Formation caps a major transgressive-regressive cycle during the Lower Cretaceous. It is the most areally extensive of three major progradational siliciclastic units in the Mississippi Interior Salt Basin (Mancini et al., 2002). **Appendix D-1** and **D-2** cross-sections show that the Paluxy Formation can be interpreted as a third order stratigraphic succession that has two major internal sequence boundaries. The Paluxy was deposited over a period of 3 million years (Mancini et al., 2002) during the Albian age. There are about 30 sandstone units in a typical vertical section of the Paluxy (**Appendix D-1** and **D-2**), which suggests that individual sandstone units have an average frequency of 100,000 years, equivalent to the Milankovitch short eccentricity cycle.

C.2 Modern Day Analogues and Depositional Model

Despite several similarities in certain elements of other braided systems, there are no modern analogs that encompass the extensive width of the Paluxy braid plain setting (~500 miles). However, several modern analogues of the Paluxy formation are proposed here from interpretations of the petrographic and geophysical data. These include: (1) The braided channel

complex and longitudinal bars of the Ganges River (**Figure C.4**); (2) The Platte River system of Nebraska; (3) the South Saskatchewan River of Canada (**Figure C.5**); and (4) Cooper's Creek, Lake Eyre Basin, central Australia (**Figure C.6**). Each system contains characteristics that share similarities with the Paluxy formation, including stratigraphic sequence, geomorphological elements, and bedload (**Figure C.3**). An understanding of reservoir composition and the formative depositional and diagenetic factors provides a predictive framework to help facilitate field-scale commercialization of anthropogenic CO_2 storage.

Figure C.4: Modern Day Analog; Google Satellite Image of the Ganges River, India

Figure C.5: Modern Day Analog; Google Satellite Image of the South Saskatchewan River, Canada

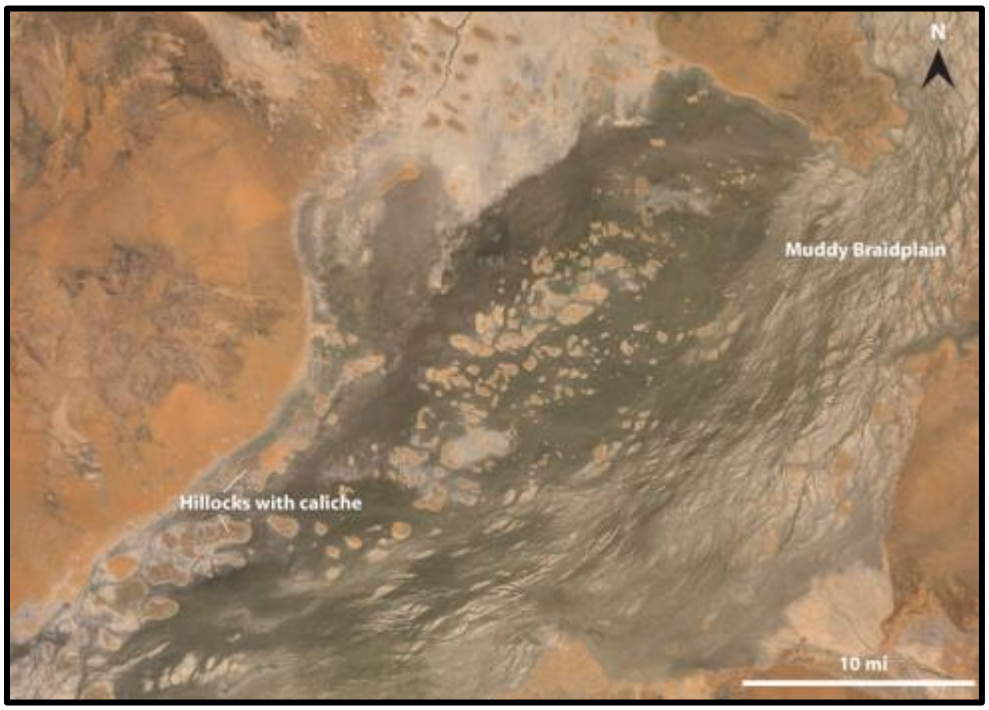

Figure C.6: Modern Day Analog; Google Satellite Image of the Cooper's Creek, Lake Eyre Basin, and Central Australia

C.3 Implications for Commercialization of CO_2 Storage Technology

Although Citronelle Field is structurally simple (**Figure C.7**), analysis of reservoir architecture (**Appendix B.1** and **B.2**) reveals extreme facies heterogeneity in the Paluxy Formation. There is abundant storage capacity and high injectivity due to high porosity and permeability in the reservoir. With so many porous and permeable sandstone units to consider in Citronelle Field, perhaps the greatest challenge for CO_2 storage programs is managing facies heterogeneity.

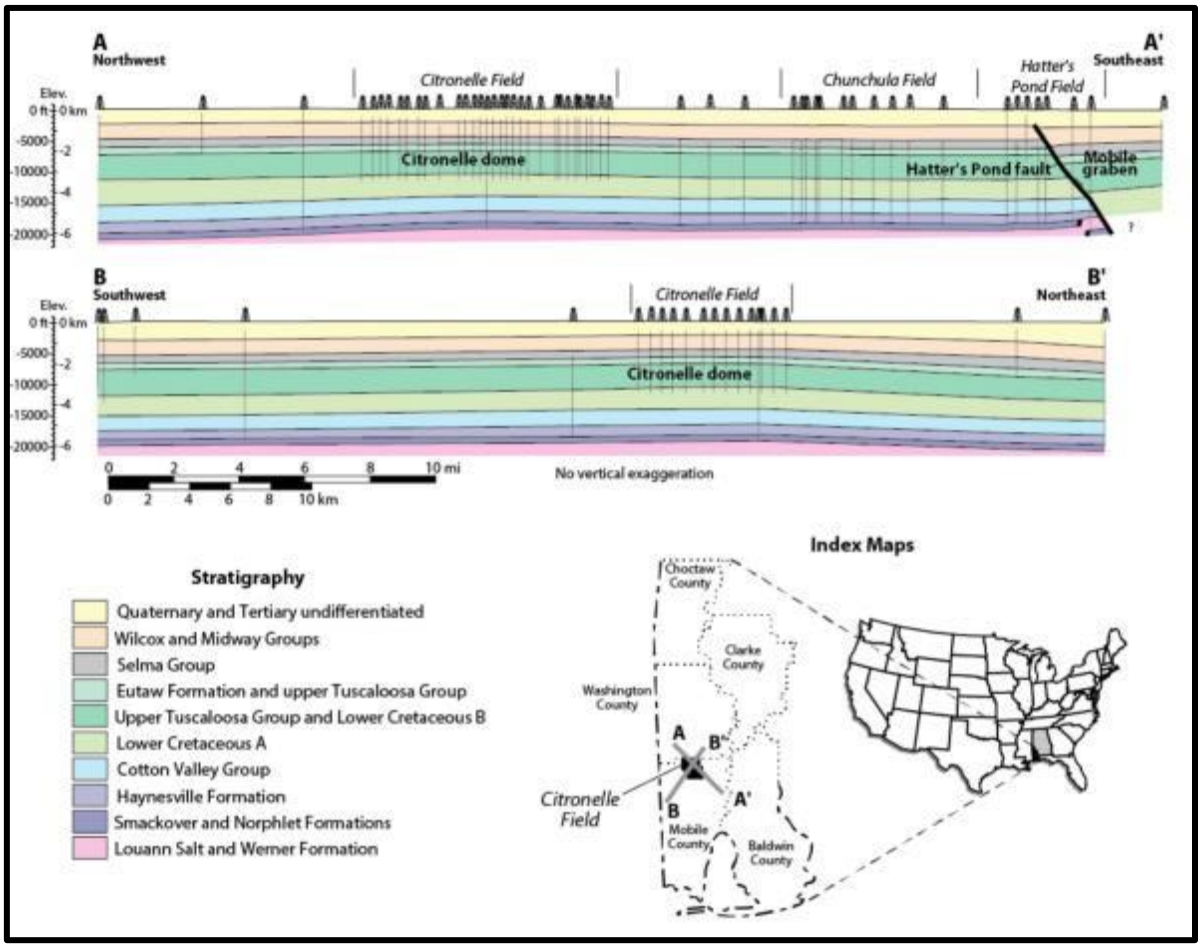

Figure C.7: Structural Cross Sections of Citronelle Dome showing Location of Citronelle Field in the Lower Cretaceous Section (From Pashin And Jin, 2004)

Stratigraphic cross sections (**Appendix B.1** and **B.2**) indicate that reservoir sandstone bodies tend to occur in clusters. Therefore, stratigraphic isolation and hydraulic confinement of the target sandstone bodies is an important factor for consideration when designing injection programs. Although there are intra-formational barriers, baffles and seals that limit the vertical migration of CO_2 plume, keeping injectate in zone may be a significant problem where successive sandstone

bodies are amalgamated into multi-storey successions, and this may limit the predictability of CO_2 flow.

Interwell heterogeneity is another key consideration in Citronelle Field. Although some sandstone units have great lateral continuity, each well may have a substantially different geophysical log signature, reflecting major variation of reservoir properties among wells (**Appendix D.1** and **D.2**).

The basal shale of the Washita-Fredericksburg, which serves as the primary seal tends to thin towards the western part of the field, with clusters of sandstone bodies overlying the seal. Care must be exercised when injecting in these areas, but the presence of numerous additional seals may reduce the risk of surface leakage of CO_2.

Primary facies heterogeneity and diagenetic processes associated with pedogenesis are the major causes of reservoir heterogeneity. Primary facies heterogeneity is expressed in the form of isolated channel fills in discontinuous sandstone units and nesting of multiple channels within widespread sandstone bodies. Pedogenesis enhances porosity through the dissolution of feldspar and the dissolution products are flushed out of the sandstone. These flushed products accumulate as clay and can plug the sandstone altering the petrophysical properties of the reservoir. It is therefore important to consider diagenetic and depositional processes, when selecting and mapping out ideal sandstone bodies with geophysical logs.

Citronelle Field is ultimately a suitable host for CO_2 sequestration and the criteria for selecting ideal sandstone bodies to inject CO_2 should not only include reservoir quality, but reservoir heterogeneity must be considered and well understood when planning injection programs.

Appendix D-1: A-A' Cross Section of the Paluxy Formation in Citronelle Field

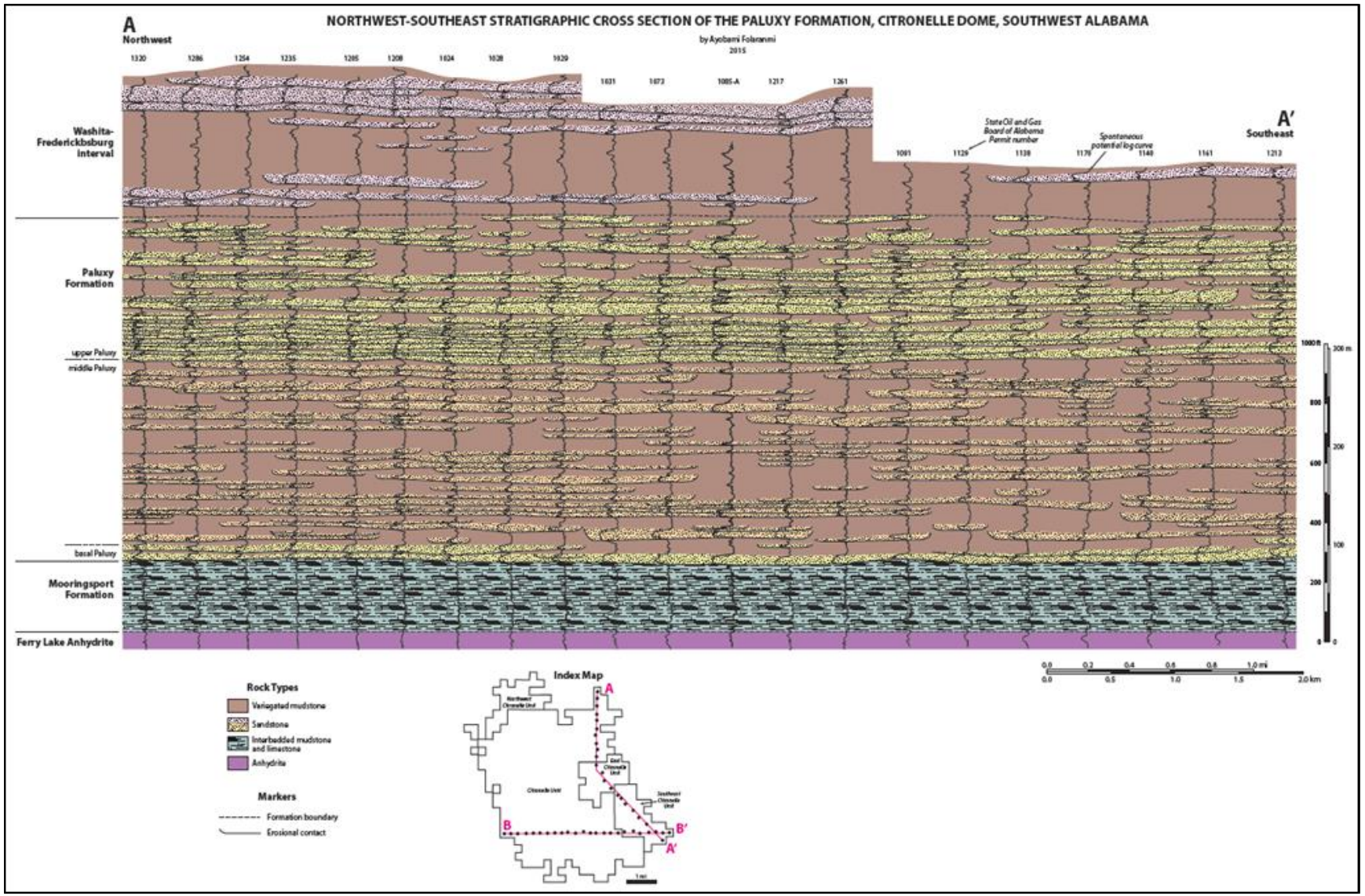

Appendix D-2: B-B' Cross Section of the Paluxy Formation in Citronelle Field